

Joint Bayesian Inference of Parameter and Discretization Error Uncertainties in ODE Models

Shoji Toyota *

toyota@ait.kyushu-u.ac.jp

Yuto Miyatake †

yuto.miyatake.cmc@osaka-u.ac.jp

abstract

We address the problem of Bayesian inference for parameters in ordinary differential equation (ODE) models based on observational data. Conventional approaches in this setting typically rely on numerical solvers such as the Euler or Runge–Kutta methods. However, these methods generally do not account for the discretization error induced by discretizing the ODE model. We propose a Bayesian inference framework for ODE models that explicitly quantifies discretization errors. Our method models discretization error as a random variable and performs Bayesian inference on both ODE parameters and variances of the randomized discretization errors, referred to as the *discretization error variance*. A key idea of our approach is the introduction of a Markov prior on the temporal evolution of the discretization error variances, enabling the inference problem to be formulated as a state-space model. Furthermore, we propose a specific form of the Markov prior that arises naturally from standard discretization error analysis. This prior depends on the step size h in the numerical solver, and we discuss its asymptotic property as $h \rightarrow +0$. Numerical experiments illustrate that the proposed method can simultaneously quantify uncertainties in both the ODE parameters and the discretization errors, and can produce posterior distributions over the parameters with broader support by accounting for discretization error.

*Department of Advanced Information Technology, Kyushu University, Japan

†D3 Center, The University of Osaka, Japan

Contents

1	Introduction	3
2	Preliminaries	5
2.1	Bayesian Inference for ODE Models	5
2.2	Discretization Error Variance	6
3	A New Approach for Joint Bayesian Inference of ODE Parameters and Discretization Error Variances	7
3.1	State-Space Model Interpretation of Discretization Error Variance Inference	7
3.1.1	Prediction Step	9
3.1.2	Correction Step	9
3.1.3	Smoothing	10
3.2	Joint Bayesian Inference of ODE Parameters and Discretization Error Variances	11
4	Markov Prior on Discretization Error Variances	14
4.1	Local Propagation of the Global Error	14
4.2	A Markov Prior	15
4.3	Asymptotics of the Prior	16
5	Experiments	17
5.1	Pendulum System	17
5.1.1	Discretization Error Quantification	18
5.1.2	Parameter Inference with Discretization Error Quantification	20
5.2	FitzHugh–Nagumo model	21
5.2.1	Discretization Error Quantification	22
5.2.2	Parameter Inference with Discretization Error Quantification	23
6	Conclusion	24
A	Derivation of Smoothing in Particle Filters	26
B	Proof of Theorem 4.1	26

1 Introduction

Ordinary differential equation (ODE) models are widely used in various scientific and engineering disciplines, including neuroscience [FitzHugh, 1961], epidemiology [Kermack and McKendrick, 1927], population biology [Volterra, 1926] and control engineering [Ogata, 2010]. These models often involve parameters that cannot be directly observed or determined; inferring such parameters from observational data is a fundamental problem. Bayesian inference is a standard approach for parameter estimation in ODE models; by placing a distribution—referred to as a *prior*—over the ODE parameter space, Bayesian inference allows us to estimate parameters in the form of a distribution known as a *posterior*. Since this posterior distribution is a probability distribution, Bayesian inference enables parameter inference along with uncertainty quantification.

One of the primary challenges in performing Bayesian inference for ODE models is the intractability of their likelihoods as they usually involve the exact solution to the ODE models. Note that standard Bayesian inference methods, such as Markov Chain Monte Carlo [Gilks et al., 1995] or variational methods [Beal, 2003], typically assume that model likelihoods are tractable; thus, this assumption is often violated in the context of ODE models. A practical strategy to address this issue involves using numerical solvers, such as Euler or Runge–Kutta methods, to approximate solutions to the ODEs [Butcher, 2016, Hairer et al., 1993]. For instance, as often employed in simulation-based inference schemes [Cranmer et al., 2020] and 4D variational (4D-Var) data assimilation [Asch et al., 2016], the likelihood is evaluated approximately by replacing the exact solution in the likelihood with a numerical solution. Another widely used method from statistics is Approximate Bayesian Computation (ABC) [Beaumont et al., 2002], which estimates the posterior distribution by comparing observations to numerical solutions obtained from numerical solvers.

These Bayesian inference methods for ODEs typically assume that numerical solvers yield sufficiently accurate solutions. However, this assumption does not always hold. For example, for chaotic systems, large-scale problems, and highly oscillatory dynamics, obtaining accurate numerical solutions remains challenging. In such settings, discretization errors may lead to biased or misleading posterior distributions (see, e.g., [Conrad et al., 2017]). This highlights the need for frameworks that can quantify the uncertainty arising from discretization errors in ODEs and to infer ODE parameters that accounts for this uncertainty.

Motivated by this objective, various methods for quantifying discretization errors have been developed, particularly within the framework of *Probabilistic Numerics* [Hennig et al., 2022]. The central idea of the framework is to interpret numerical computation as a statistical inference, enabling a principled quantification of discretization uncertainty. A well-established example is Bayesian ODE solvers [Beck et al., 2024, Kersting et al., 2020, Le Fay et al., 2025, Schmidt et al., 2021, Schober et al., 2018, Tronarp et al., 2022, 2019, 2021], which reformulate the numerical solution of ODEs as a Gaussian process inference problem, in contrast to traditional deterministic solvers. Another prominent line is perturbative approaches [Abdulle and Garegnani, 2020, Conrad et al., 2017, Lie et al., 2022, 2019], which compute numerical solutions together with probabilistic perturbations.

A distinct class of discretization error quantification methods for ODEs is the *discretization error variance* approach [Marumo et al., 2024, Matsuda and Miyatake, 2021, Miyatake et al., 2025]. In this framework, standard numerical solvers such as the Runge–Kutta method are employed to solve ODEs, and

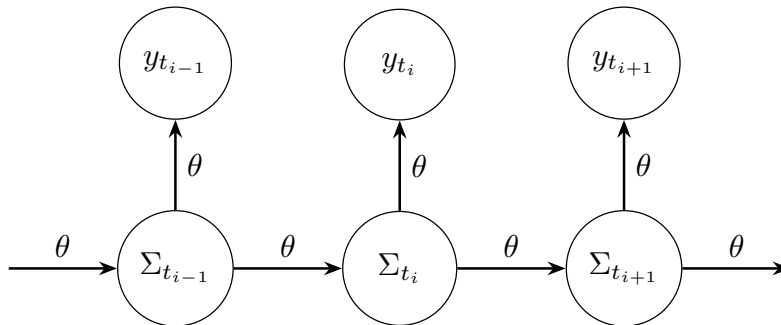


Figure 1: Our state-space modeling formulation. Let y_t , θ , and Σ_t denote the observation, the ODE parameter, and the discretization error variance, respectively (their formal definitions are provided in the next section). By placing a Markov prior on the discretization error variances Σ_{t_i} , we obtain a state-space model in which the latent variables correspond to the discretization error variances. The ODE parameters θ govern both the latent transition $\Sigma_{t_i} \rightarrow \Sigma_{t_{i+1}}$ and the observation process $\Sigma_{t_i} \rightarrow y_{t_i}$.

the discretization errors introduced by these solvers are modeled as random variables. Their variances—referred to as *discretization error variances*—are treated as statistical quantities to be inferred from observations. A key distinction between this approach and those described above is that the discretization error itself is inferred directly from observations. Another important feature is that insights from classical error analysis can be incorporated into the modeling of the discretization error variance. For example, Marumo et al. [2024], Matsuda and Miyatake [2021], Miyatake et al. [2025] imposed a monotonicity constraint on the discretization error variance, reflecting the well-known principle from numerical analysis that numerical errors tend to accumulate over time. However, within this context, a Bayesian framework that simultaneously infers both the model parameters and the discretization error variance remains undeveloped.

In this study, we propose a Bayesian inference framework for jointly estimating ODE parameters and discretization errors, building upon the discretization error variance approach. By adopting a fully Bayesian perspective, we place priors not only on the ODE parameters but also on the discretization error variances, thereby enabling joint uncertainty quantification of both ODE parameters and discretization errors.

A key feature of our framework is to set a prior over the time course of the discretization error variances that satisfies the markov property. By imposing a markov property on a prior, our objectives can be formulated as an inference on state-space models, in which the discretization error variances, observations, and ODE parameters correspond to the latent variables, observation variables, and parameters of the state-space model, respectively (Figure 1). In state-space modeling, various methodologies have been developed for estimating the posterior distributions of latent states together with parameters in a state-space model; by leveraging them, we are able to perform joint Bayesian inference on both the discretization error variances and the ODE parameters. In particular, we employ particle filtering [Doucet et al., 2001, Gordon et al., 1993, Kitagawa, 1996], in combination with a self-organizing technique [Kitagawa, 1998], to obtain the posterior over discretization error variances and ODE parameters.

The specification of a Markov prior over the discretization error variances is crucial for ensuring the

effectiveness of the proposed method. In this paper, we propose a Markov prior inspired by the standard discretization error analysis of ordinary differential equations (ODEs). In numerical analysis, it is well known that the discretization error can be represented by the accumulation of local errors, the errors incurred at each individual step. From this viewpoint, we introduce a Markov prior in which the local truncation errors accumulate additively over time. We further investigate theoretical properties of the proposed prior; in particular, since the prior depends on the step size of the solver used to obtain the numerical solution, we analyze the asymptotic behavior of the proposed prior as the step size approaches zero.

The paper is organized as follows. Section 2 provides background for this research. In Section 3, we present the proposed method. Specifically, we first reformulate the inference of discretization error variances as a state-space modeling problem (Subsection 3.1). We then extend this framework to the joint Bayesian inference of both discretization error variances and ODE parameters using a self-organizing state-space model (Subsection 3.2). In Section 4, we construct a Markov prior for discretization error variances motivated by principles from numerical error analysis and establish an asymptotic property of the proposed prior as the step size goes to zero. Section 5 demonstrates the effectiveness of our method through numerical experiments on the pendulum system and the FitzHugh–Nagumo model. Finally, Section 6 summarizes our contributions and discusses directions for future work.

2 Preliminaries

2.1 Bayesian Inference for ODE Models

Consider a $d_{\mathcal{X}}$ -dimensional ordinary differential equation (ODE):

$$\frac{dx(t)}{dt} = f(x(t; \theta), \theta), \quad (1)$$

where the initial condition $x(0; \theta)$ and the solution $x(t; \theta)$ lie in $\mathbb{R}^{d_{\mathcal{X}}}$ with $d_{\mathcal{X}} \in \mathbb{N}_{>0}$. Here $\theta \in \mathbb{R}^d$ is an unknown parameter that should be estimated. The function f is defined as $f : \mathbb{R}^{d_{\mathcal{X}}} \times \mathbb{R}^d \rightarrow \mathbb{R}^{d_{\mathcal{X}}}$. We assume that noisy observations $y_{t_0}^*, \dots, y_{t_N}^* \in \mathbb{R}^{d_{\mathcal{Y}}}$ of the true trajectory $x(t; \theta^*)$ are available at discrete time points $0 \leq t_0 < \dots < t_N$, where

$$y_{t_i}^* = Hx(t_i; \theta^*) + \varepsilon_i. \quad (2)$$

Here, the linear observation operator $H \in \mathbb{R}^{d_{\mathcal{Y}} \times d_{\mathcal{X}}}$ is a full rank matrix, and observation noises $\varepsilon_i \sim \mathcal{N}(0, \Gamma)$ are drawn i.i.d. from a multivariate normal distribution with an invertible covariance matrix Γ .

A principled approach to inferring the ODE parameter from observations $y_{t_0}^*, \dots, y_{t_N}^*$ is Bayesian inference. Given a likelihood $p(y_{t_0}, \dots, y_{t_N} \mid \theta)$ and a prior distribution $p(\theta)$, Bayesian inference aims to compute the posterior distribution:

$$p(\theta \mid y_{t_0}^*, \dots, y_{t_N}^*) \propto p(y_{t_0}^*, \dots, y_{t_N}^* \mid \theta) \cdot p(\theta).$$

Traditional Bayesian inference methods, such as Markov Chain Monte Carlo (MCMC) [Gilks et al., 1995]

and variational inference [Beal, 2003], require access to an analytical form of the likelihood:

$$\begin{aligned}
 p(y_{t_0}, \dots, y_{t_N} | \theta) &= \prod_{i=0}^N p(y_{t_i} | \theta) \\
 &= \prod_{i=0}^N \frac{1}{\sqrt{(2\pi)^{d_y} |\Gamma|}} \exp \left\{ -\frac{1}{2} (y_{t_i} - Hx(t_i; \theta))^T \Gamma^{-1} (y_{t_i} - Hx(t_i; \theta)) \right\},
 \end{aligned}$$

where $x(t_i; \theta)$ denotes the solution of the ODE at time t_i given ODE parameter θ .

However, evaluating this likelihood is often intractable as the exact solution $x(t_i; \theta)$ is inaccessible. Although numerical solvers such as Runge–Kutta or Euler methods are commonly employed, numerical solutions $x_{t_i}(\theta) \approx x(t_i; \theta)$ inevitably deviate from the true trajectory $x(t_i; \theta)$ due to discretization errors. These errors introduce bias into the likelihood, which can significantly affect inference accuracy. To address this issue, several methods have been proposed to statistically quantify discretization errors. Well-known examples include Bayesian ODE solvers [Beck et al., 2024, Bosch et al., 2024, Kersting et al., 2020, Le Fay et al., 2025, Schmidt et al., 2021, Schober et al., 2018, Tronarp et al., 2022, 2019, 2021] and perturbative methods [Abdulle and Garegnani, 2020, Conrad et al., 2017, Lie et al., 2022, 2019], both of which fall within the category of *Probabilistic Numerics* [Hennig et al., 2022].

2.2 Discretization Error Variance

In the next section, we present a Bayesian inference method for estimating the ODE parameter θ that explicitly accounts for discretization errors. Our discussion builds on the recently proposed concept of *discretization error variance* [Marumo et al., 2024, Matsuda and Miyatake, 2021, Miyatake et al., 2025]. The central idea of this concept is summarized as follows.

In contrast to Bayesian ODE solvers and perturbative methods, we explicitly model the discretization errors induced by a numerical solver as random variables. Specifically, the discretization error at $t = t_i$:

$$r_{t_i} = x(t_i; \theta) - x_{t_i}(\theta)$$

is assumed to follow a Gaussian distribution

$$r_{t_i} \sim \mathcal{N}(0, \Sigma_{t_i}). \tag{3}$$

Here, the covariance matrix Σ_{t_i} , referred to as the *discretization error variance*, is treated as a statistical quantity to be inferred from observations and numerical solutions, thereby providing a way to quantify the discretization error. Equivalently, the exact solution $x(t_i; \theta)$ can also be interpreted as a random variable:

$$x(t_i; \theta) \sim \mathcal{N}(x_{t_i}(\theta), \Sigma_{t_i}), \tag{4}$$

where $x_{t_i}(\theta)$ denotes a numerical approximation.

Under this framework, we obtain a modified likelihood

$$\begin{aligned}
p(y_{t_0}, \dots, y_{t_N} \mid \theta, \Sigma_{t_1}, \dots, \Sigma_{t_N}) &= \prod_{i=0}^N p(y_{t_i} \mid \Sigma_{t_i}, \theta) \\
&= \prod_{i=0}^N \frac{1}{\sqrt{(2\pi)^{d_y} |\Gamma + V_{t_i}|}} \exp \left\{ -\frac{1}{2} (y_{t_i} - Hx_{t_i}(\theta))^\top (\Gamma + V_{t_i})^{-1} (y_{t_i} - Hx_{t_i}(\theta)) \right\}
\end{aligned} \tag{5}$$

with $V_{t_i} = H \cdot \Sigma_{t_i} \cdot H^\top$, which will also be referred to as the discretization error variance. A central feature of this framework is to infer the ODE parameters and the discretization error variances simultaneously.

3 A New Approach for Joint Bayesian Inference of ODE Parameters and Discretization Error Variances

In this study, we aim to develop a method for performing Bayesian inference for ODE parameters while accounting for discretization errors introduced by numerical solvers. Specifically, we focus on the ODE parameters θ and the discretization error variances Σ_{t_i} .

Given a prior distribution $p(\theta, \Sigma_{t_0}, \dots, \Sigma_{t_N})$ on ODE parameters θ and discretization error variances Σ_{t_i} , our target is to obtain the posterior distribution

$$p(\theta, \Sigma_{t_0}, \dots, \Sigma_{t_N} \mid y_{t_0}, \dots, y_{t_N}) \propto p(y_{t_0}, \dots, y_{t_N} \mid \theta, \Sigma_{t_0}, \dots, \Sigma_{t_N}) \cdot p(\theta, \Sigma_{t_0}, \dots, \Sigma_{t_N}). \tag{6}$$

The key components of this framework are the specification of the prior $p(\theta, \Sigma_{t_0}, \dots, \Sigma_{t_N})$ and the construction of an algorithm for sampling from the posterior distribution. In this section, we outline the general ideas underlying the prior and the sampling scheme. A specific form of the prior will be discussed in the next section, noting that some flexibility in its choice remains.

We note that this form of joint Bayesian inference has not been explored in the literature on discretization error variance. Previous studies either perform point estimation of the ODE parameters and discretization error variances [Marumo et al., 2024, Matsuda and Miyatake, 2021], or conduct Bayesian inference only for discretization error variances, without jointly inferring the ODE parameters [Miyatake et al., 2025].

3.1 State-Space Model Interpretation of Discretization Error Variance Inference

To illustrate our core idea clearly, we first focus on the Bayesian inference of the discretization error variances Σ_{t_i} alone. In this setting, in stead of the original objective (6), our target is the posterior distribution

$$p(\Sigma_{t_0}, \dots, \Sigma_{t_N} \mid y_{t_0}, \dots, y_{t_N}) \propto p(y_{t_0}, \dots, y_{t_N} \mid \Sigma_{t_0}, \dots, \Sigma_{t_N}) \cdot p(\Sigma_{t_0}, \dots, \Sigma_{t_N}), \tag{7}$$

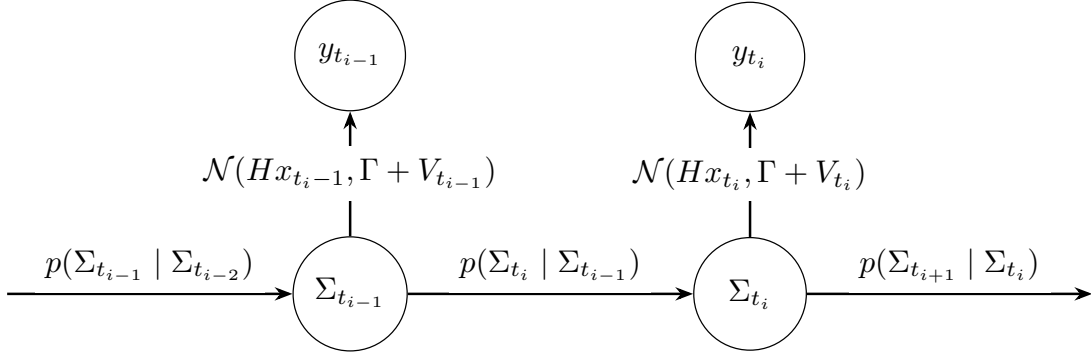


Figure 2: Reduction of our objective (7) to a state-space model. Its latent transition and observation process are given by a markov prior $p(\Sigma_{t_{i+1}} | \Sigma_{t_i})$ and $\mathcal{N}(Hx_{t_i}, V_{t_i} + \Gamma)$ respectively.

which concerns only the discretization error variances $(\Sigma_{t_0}, \dots, \Sigma_{t_N})$. The joint inference (6) of ODE parameters and discretization error variances will be discussed in Section 3.2.

In our approach, we interpret the discretization error variances as latent variables and the observations y_i as observation variables in a corresponding state-space model. Under this formulation, posterior sampling can be performed using a filtering-based approach.¹

Specifically, we assume a Markovian structure for the prior distribution over the discretization error variances:

$$\Sigma_{t_0} \rightarrow \Sigma_{t_1} \rightarrow \dots \rightarrow \Sigma_{t_N}.$$

Under this Markov property, the discretization error variances and the observations form a state-space model, as illustrated in Figure 2. Here, the latent transition $\Sigma_{t_i} \rightarrow \Sigma_{t_{i+1}}$ corresponds to the Markov prior $p(\Sigma_{t_{i+1}} | \Sigma_{t_i})$ over the discretization error variances, while the observation process $\Sigma_{t_i} \rightarrow y_{t_i}$ is given by

$$p(y_{t_i} | \Sigma_{t_i}) = \frac{1}{\sqrt{(2\pi)^{d_y} |\Gamma + V_{t_i}|}} \exp \left\{ -\frac{1}{2} (y_{t_i} - Hx_{t_i})^\top (\Gamma + V_{t_i})^{-1} (y_{t_i} - Hx_{t_i}) \right\}, \quad (8)$$

which is a multivariate normal distribution with mean given by the numerical solution x_{t_i} at time t_i and covariance $\Gamma + V_{t_i}$. Here, V_{t_i} is defined by $V_{t_i} = H \cdot \Sigma_{t_i} \cdot H^\top$.

For the posterior sampling, we primarily employ the particle filter [Doucet et al., 2001, Gordon et al., 1993, Kitagawa, 1996], as detailed in Algorithm 1. Hereafter, the tuples $\{y_{t_0}, \dots, y_{t_i}\}$ and $\{\Sigma_{t_0}, \dots, \Sigma_{t_i}\}$ are often abbreviated by $y_{0:i}$ and $\Sigma_{0:i}$ respectively. The particle filter approximates the posterior distribution $p(\Sigma_{t_i} | y_{0:i}^*)$ by a finite sum $\frac{1}{K} \sum_{k=0}^K \delta_{\Sigma_{i|0:i}^k}$, where $\delta_{\Sigma_{i|0:i}^k}$ denotes the Dirac measure at the discrete point $\Sigma_{i|0:i}^k$, and each $\Sigma_{i|0:i}^k$ is called a *particle*. Given K particles $\{\Sigma_{i|0:i}^k\}_{k=1}^K$ representing $p(\Sigma_{t_i} | y_{0:i}^*)$, the particles $\{\Sigma_{i+1|0:i+1}^k\}_{k=0}^K$ of $p(\Sigma_{t_{i+1}} | y_{0:i+1}^*)$ at the next time step t_{i+1} are recursively obtained through the *prediction* and *correction* steps (see Sections 3.1.1 and 3.1.2). Finally, particles representing the target

¹The introduction of a Markov prior is also a key component in Bayesian ODE solvers for reducing computational costs [Beck et al., 2024, Bosch et al., 2024, Cockayne et al., 2019, Schmidt et al., 2021, Tronarp et al., 2022]. The essential difference, however, is that Bayesian ODE solvers place a Markov prior on solutions of the differential equation itself, whereas in this study the Markov prior is placed on trajectories of the discretization errors. As will be discussed in the next section, imposing a prior distribution directly on the discretization error allows insights from classical error analysis to be incorporated into the prior—something that is difficult to achieve when the prior is placed on the solution itself.

Algorithm 1 Particle Filter for Bayesian Inference on Σ_{t_i}

- 1: **Input:** A prior $p(\Sigma_{t_0}) \prod_{i=0}^{N-1} p(\Sigma_{t_{i+1}} | \Sigma_{t_i})$, observations $y_{0:N}^*$,
A differential equation $\frac{dx(t)}{dt} = f(x(t))$ with a numerical solver
- 2: Randomly generate K particles $\{\Sigma_{0|0:0}^k\}_{k=1}^K \sim p(\Sigma_{t_0})$ // Generate Particles at Time t_0
- 3: **for** $i = 0$ to $N - 1$ **do**
- 4: $\{\Sigma_{i+1|0:i}^k\}_{k=1}^K \sim p(\Sigma_{t_{i+1}} | \Sigma_{i|0:i}^k)$ // Prediction Step
- 5: Solve $\frac{dx(t)}{dt} = f(x(t), \theta)$ to obtain a numerical solution $x_{t_{i+1}}$.
- 6: For each k , evaluate $p(y_{t_{i+1}}^* | \Sigma_{i+1|0:i}^k)$ with $x_{t_{i+1}}$, and obtain

$$w_k := \frac{p(y_{t_{i+1}}^* | \Sigma_{i+1|0:i}^k)}{\sum_{k=1}^K p(y_{t_{i+1}}^* | \Sigma_{i+1|0:i}^k)} \quad // \text{ Correction Step}$$

- 7: $\text{re}_1, \dots, \text{re}_K \sim \text{Categorical}(w_1, \dots, w_K)$.
- 8: Update particles by

$$\Sigma_{i+1|0:i+1}^k := \Sigma_{i+1|0:i}^{\text{re}_k} \quad // \text{ Resampling}$$

$$\Sigma_{0|0:0}^k = \Sigma_{1|0:0}^{\text{re}_k}, \dots, \Sigma_{j|0:j}^k = \Sigma_{j|0:j}^{\text{re}_k}, \dots, \Sigma_{i|0:i}^k = \Sigma_{i|0:i}^{\text{re}_k}. \quad // \text{ Smoothing}$$

9: **end for**

- 10: **Output:** Particles $\left\{ \left(\Sigma_{0|0}^k, \dots, \Sigma_{N|0:N}^k \right) \right\}_{k=1}^K$ of $p(\Sigma_{0:N} | y_{0:N}^*)$.
-

distribution $p(\Sigma_{0:N} | y_{0:N}^*)$ are obtained via the *smoothing* step (see Section 3.1.3).

Before detailing each step, we emphasize that while evaluating the modified likelihood (8) is straightforward, it is crucial to choose the Markov prior $p(\Sigma_{t_{i+1}} | \Sigma_{t_i})$ such that sampling from it can be performed efficiently (the selection will be discussed in Section 4).

3.1.1 Prediction Step

Assume that we have the particles $\{\Sigma_{i|0:i}^k\}_{k=1}^K$ approximating the distribution $p(\Sigma_{t_i} | y_{0:i}^*)$. Then, the particles $\{\Sigma_{i+1|0:i}^k\}_{k=1}^K$ approximating $p(\Sigma_{t_{i+1}} | y_{0:i}^*)$ can be generated through

$$\Sigma_{i+1|0:i}^k \sim p(\Sigma_{t_{i+1}} | \Sigma_{i|0:i}^k),$$

that is, by sampling from the Markov prior $p(\Sigma_{t_{i+1}} | \Sigma_{t_i})$ with the conditioning $\Sigma_{t_i} = \Sigma_{i|0:i}^k$.

3.1.2 Correction Step

Given new observation $y_{t_{i+1}}^*$ at the next time t_{i+1} , this step generates particles $\{\Sigma_{i+1|0:i+1}^k\}_{k=1}^K$ that estimate

$$p(\Sigma_{t_{i+1}} | y_{0:i}^*, y_{t_{i+1}}^*) = p(\Sigma_{t_{i+1}} | y_{0:i+1}^*) \propto p(y_{t_{i+1}}^* | \Sigma_{t_{i+1}}) \cdot p(\Sigma_{t_{i+1}} | y_{0:i}^*). \quad (9)$$

Recall that in the previous prediction step, we obtained a particle approximation $\{\Sigma_{i+1|0:i}^k\}_{k=1}^K$ of the distribution $p(\Sigma_{t_{i+1}} | y_{0:i}^*)$. Therefore, the distribution $p(\Sigma_{t_{i+1}} | y_{0:i+1}^*)$ can be approximated as

$$p(\Sigma_{t_{i+1}} | y_{0:i+1}^*) \propto p(y_{i+1}^* | \Sigma_{t_{i+1}}) \cdot p(\Sigma_{t_{i+1}} | y_{0:i}^*) \approx \sum_{k=1}^K w_k \delta_{\Sigma_{i+1|0:i}^k},$$

where the weights w_k are defined as

$$w_k := \frac{p(y_{i+1}^* | \Sigma_{i+1|0:i}^k)}{\sum_{\bar{k}=1}^K p(y_{i+1}^* | \Sigma_{i+1|0:i}^{\bar{k}})}. \quad (10)$$

We then perform *resampling* to equalize the particle weights w_i [Kitagawa, 1996, Gordon et al., 1993]. Specifically, K indices $\text{re}_1, \dots, \text{re}_K \in \{1, \dots, K\}$ are sampled from $\text{Categorical}(w_1, \dots, w_K)$, i.e., the distribution in which index $k \in \{1, \dots, K\}$ is selected with probability w_k . Then, the particles are subsequently updated as

$$\Sigma_{i+1|0:i+1}^k := \Sigma_{i+1|0:i}^{\text{re}_k}. \quad (11)$$

This procedure yields a new particle set $\{\Sigma_{i+1|0:i+1}^k\}_{k=1}^K$ with uniform weights, which approximates the posterior $p(\Sigma_{t_{i+1}} | y_{0:i+1}^*)$.

Remark 1. It is well known that the resampling procedure gradually reduces particle diversity over time: this phenomenon is commonly referred to as *particle degeneracy*. This issue becomes particularly severe in high-dimensional latent spaces, where the posterior distribution must be represented by a limited number of particles. Various strategies have been proposed to mitigate this problem. One such method is the *merging particle filter* [Nakano et al., 2007, Van Leeuwen, 2009], in which multiple particles are generated and then merged to form a single representative particle. Another approach is the *localized particle filter* [Farchi and Bocquet, 2018, Van Leeuwen et al., 2019], based on the assumption that observations depend only on a subset of the latent state. Additional variants include the *tempering particle filter* [Beskos et al., 2014], which employs tempering techniques [Neal, 1996, Del Moral et al., 2006], and the *implicit particle filter* [Atkins et al., 2013, Chorin et al., 2010], which alleviates degeneracy through the design of appropriate proposal distributions. Since the primary objective of the present paper is to illustrate an approach for inferring ODE parameters with discretization error quantification within the framework of state-space modelling, rather than to propose a new filtering algorithm, the standard particle filter is employed; nonetheless, the enhanced variants mentioned above could also be utilized.

3.1.3 Smoothing

In the operations described so far, the particles $\{\Sigma_{i|0:i}^k\}_{k=1}^K$ obtained at times $t_i = t_0, \dots, t_{N-1}$ are sampled from $p(\Sigma_{t_i} | y_{0:i}^*)$ rather than from the distribution that incorporates all future observations, $p(\Sigma_{t_i} | y_{0:N}^*)$. This limitation is addressed by a procedure known as *smoothing*.

In a particle filter, a principled way to perform smoothing is to update

$$\Sigma_{0|0:0}^k := \Sigma_{0|0:0}^{\text{re}_k}, \dots, \Sigma_{j|0:j}^k := \Sigma_{j|0:j}^{\text{re}_k}, \dots, \Sigma_{i|0:i}^k := \Sigma_{i|0:i}^{\text{re}_k}, \quad (12)$$

in the resampling step (11), together with $\Sigma_{i+1|0:i+1}^k := \Sigma_{i+1|0:i}^{\text{rek}}$. Through this operation, the particles $\Sigma_{j|0:j}^k$ ($0 \leq j \leq i$) become samples from $p(\Sigma_{t_j} | y_{0:i+1}^*)$, which incorporates the observations $y_{t_0}^*, \dots, y_{t_{i+1}}^*$ beyond time j [Kitagawa, 1996] (see Appendix A for details). By repeating this procedure until $i = N-1$, the resulting particles $\Sigma_{j|0:j}^k$ approximate draws from $p(\Sigma_{t_j} | y_{0:N}^*)$.

Remark 2. The resampling procedure (12) simultaneously updates the weight indices for all time steps, thereby reducing the particle diversity even at early stages ($j \ll N$). One way to mitigate this issue is *fixed-lag smoothing* [Kitagawa, 1996], in which resampling is restricted to only the past L steps:

$$\Sigma_{i-L|0:i-L}^k = \Sigma_{i-L|0:i-L}^{\text{rek}}, \dots, \Sigma_{i|0:i}^k = \Sigma_{i|0:i}^{\text{rek}}. \quad (13)$$

This approach confines particle degeneration due to resampling to the most recent L time steps. In addition, the various resampling techniques introduced in the previous section to mitigate particle degeneration can also be applied here to further suppress their effects during smoothing.

3.2 Joint Bayesian Inference of ODE Parameters and Discretization Error Variances

We return to our objective (6)—obtaining the posterior $p(\theta, \Sigma_{t_0}, \dots, \Sigma_{t_N} | y_{t_0}, \dots, y_{t_N})$ over both the discretization error variances Σ_{t_i} and the ODE parameter θ .

We now reformulate our target posterior distribution (6) as a state-space modeling problem, based on the discussion in the previous section. First, we introduce a conditional Markov prior $p(\theta, \Sigma_{t_0}, \dots, \Sigma_{t_N})$ over $(\theta, \Sigma_{t_0}, \dots, \Sigma_{t_N})$, in which the sequence $(\Sigma_{t_0}, \dots, \Sigma_{t_N})$ satisfies the Markov property conditioned on the model parameter θ :

$$p(\theta, \Sigma_{t_0}, \dots, \Sigma_{t_N}) = p(\theta) \cdot p(\Sigma_{t_0} | \theta) \prod_{i=0}^{N-1} p(\Sigma_{t_{i+1}} | \Sigma_{t_i}, \theta).$$

As the likelihood $p(y_{t_0}, \dots, y_{t_N} | \theta, \Sigma_{t_0}, \dots, \Sigma_{t_N})$ can be factorized as $\prod_{i=0}^N p(y_{t_i} | \theta, \Sigma_{t_i})$ in (5), the joint model $p(y_{t_0}, \dots, y_{t_N}, \theta, \Sigma_{t_0}, \dots, \Sigma_{t_N})$ can be expressed as

$$\begin{aligned} p(y_{t_0}, \dots, y_{t_N}, \theta, \Sigma_{t_0}, \dots, \Sigma_{t_N}) &= p(y_{t_0}, \dots, y_{t_N} | \theta, \Sigma_{t_0}, \dots, \Sigma_{t_N}) \cdot p(\theta, \Sigma_{t_0}, \dots, \Sigma_{t_N}) \\ &= \left(\prod_{i=0}^N p(y_{t_i} | \Sigma_{t_i}, \theta) \right) \left(p(\theta) \cdot p(\Sigma_{t_0} | \theta) \prod_{i=0}^{N-1} p(\Sigma_{t_{i+1}} | \Sigma_{t_i}, \theta) \right) \\ &= \underbrace{p(\theta)}_{(*)} \cdot \underbrace{\left(p(\Sigma_{t_0} | \theta) \cdot \prod_{i=0}^N p(y_{t_i} | \Sigma_{t_i}, \theta) \cdot \prod_{i=0}^{N-1} p(\Sigma_{t_{i+1}} | \Sigma_{t_i}, \theta) \right)}_{(**)}. \end{aligned}$$

Thus, the joint model $p(y_{t_0}, \dots, y_{t_N}, \theta, \Sigma_{t_0}, \dots, \Sigma_{t_N})$ consists of a state-space model (**), where both the latent state transitions $p(\Sigma_{t_{i+1}} | \Sigma_{t_i}, \theta)$ and the observation model $p(y_{t_i} | \Sigma_{t_i}, \theta)$ depend on the model parameter θ , together with a prior distribution $p(\theta)$ (*) (see Figure 1). Here, the observation process

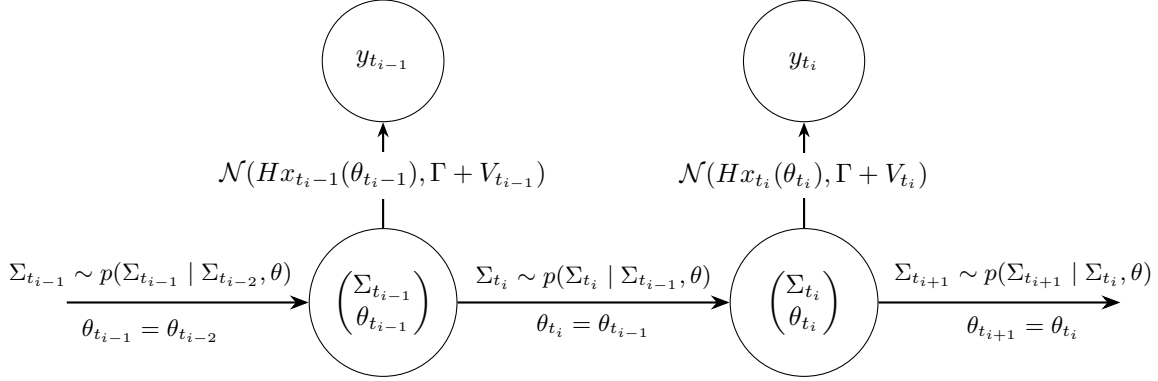


Figure 3: Self-organizing state-space modeling to perform joint Bayesian inference of the latent state Σ_{t_i} and the ODE parameters θ shown in Figure 1. In this method, we construct an augmented state-space model by considering the joint latent state $(\Sigma_{t_i}, \theta_{t_i})^\top$, and define its transition as $\Sigma_{t_{i+1}} \sim p(\Sigma_{t_{i+1}} | \Sigma_{t_i}, \theta)$ and $\theta_{t_{i+1}} = \theta_{t_i}$. By solving this alternative state-space model using a particle filter, we obtain the desired posterior distribution (6).

$p(y_{t_i} | \Sigma_{t_i}, \theta)$ is given by

$$\begin{aligned}
 p(y_{t_i} | \Sigma_{t_i}, \theta) &:= \mathcal{N}(Hx_{t_i}(\theta), \Gamma + V_{t_i}) \\
 &= \frac{1}{\sqrt{(2\pi)^{d_Y} |\Gamma + V_{t_i}|}} \exp \left\{ -\frac{1}{2} (y_{t_i} - Hx_{t_i}(\theta))^\top (\Gamma + V_{t_i})^{-1} (y_{t_i} - Hx_{t_i}(\theta)) \right\}, \quad (14)
 \end{aligned}$$

which is a modified version of the observation process (8) and compatible to the modified likelihood (5) where the numerical solution $x_{t_i}(\theta)$ explicitly depends on the model parameter θ . This reformulation implies that inferring the posterior $p(\theta, \Sigma_{t_0}, \dots, \Sigma_{t_N} | y_{t_0}, \dots, y_{t_N})$ in (6) can be cast as a joint Bayesian inference problem for the latent states Σ_{t_i} and the model parameter θ in the state-space model (**).

Since we have reformulated our objective (6) as a joint Bayesian inference for the latent states and model parameters within a state-space model, we can exploit existing methods developed for such joint inference in the context of the filtering approach. A well-known method of this kind is the *self-organizing state-space model* [Kitagawa, 1998], which is summarized in Algorithm 2. In this method, an alternative state-space formulation, as illustrated in Figure 3, is considered, in which the model parameter θ is incorporated into the latent state Σ_{t_i} by introducing the augmented latent variable

$$\hat{\Sigma}_{t_i} = \begin{pmatrix} \Sigma_{t_i} \\ \theta_{t_i} \end{pmatrix},$$

where the parameters θ are formally treated as time-varying variables θ_{t_i} with constant transition $\theta_{t_{i+1}} = \theta_{t_i}$, even though they are originally time-invariant. We define a Markov distribution over $\hat{\Sigma}_{t_i}$ by initializing

$$\hat{\Sigma}_{t_0} = (\Sigma_{t_0}, \theta_{t_0})^\top \sim p(\Sigma_{t_0} | \theta) \cdot p(\theta)$$

Algorithm 2 Particle Filter for Bayesian Inference on Σ_{t_i} and θ

- 1: **Input:** A prior $p(\theta, \Sigma_{0:N}) = p(\theta) \cdot p(\Sigma_{t_0} | \theta) \prod_{i=0}^{N-1} p(\Sigma_{t_{i+1}} | \Sigma_{t_i}, \theta)$, observations $y_{0:N}^*$,
A differential equation $\frac{dx(t)}{dt} = f(x(t), \theta)$ with a numerical solver
- 2: Generate particles $\left\{ \left(\Sigma_{0|0:0}^k, \theta_{0|0:0}^k \right) \right\}_{k=1}^K \sim p(\Sigma_{t_0} | \theta) \cdot p(\theta)$ // Generate Particles at Time t_0
- 3: **for** $i = 0$ to $N - 1$ **do**
- 4: Generate particles $\left\{ \left(\Sigma_{i+1|0:i}^k, \theta_{i+1|0:i}^k \right) \right\}_{k=1}^K$ by
 $\Sigma_{i+1|0:i}^k \sim p(\Sigma_{t_{i+1}} | \Sigma_{t_i}^k), \quad \theta_{i+1|0:i}^k := \theta_{i|0:i}^k$ // Prediction Step
- 5: For each k , solve $\frac{dx(t)}{dt} = f(x(t), \theta_{i+1|0:i}^k)$ to obtain a numerical solution $x_{t_{i+1}}(\theta_{i+1|0:i}^k)$.
- 6: For each k , evaluate $p(y_{i+1}^* | \Sigma_{i+1|0:i}^k, \theta_{i+1|0:i}^k)$ with $x_{t_{i+1}}(\theta_{i+1|0:i}^k)$ and obtain

$$w_k := \frac{p(y_{i+1}^* | \Sigma_{i+1|0:i}^k, \theta_{i+1|0:i}^k)}{\sum_{k=1}^K p(y_{i+1}^* | \Sigma_{i+1|0:i}^k, \theta_{i+1|0:i}^k)} \quad // \text{Correction Step}$$

- 7: $re_1, \dots, re_K \sim \text{Categorical}(w_1, \dots, w_K)$.
- 8: Update particles by

$$\Sigma_{i+1|0:i+1}^k := \Sigma_{i+1|0:i}^{re_k}, \quad \theta_{i+1|0:i+1}^k := \theta_{i+1|0:i}^{re_k} \quad // \text{Resampling}$$

$$\Sigma_{0|0:0}^k = \Sigma_{1|0:1}^{re_k}, \dots, \Sigma_{j|0:j}^k = \Sigma_{j|0:j}^{re_k}, \dots, \Sigma_{i|0:i}^k = \Sigma_{i|0:i}^{re_k}. \quad // \text{Smoothing}$$

9: **end for**

- 10: **Output:** Particles $\left\{ \left(\theta_{N|0:N}^k, \Sigma_{0|0}^k, \dots, \Sigma_{N|0:N}^k \right) \right\}_{k=1}^K$ of $p(\theta, \Sigma_{0:N} | y_{0:N}^*)$.
-

at the initial time t_0 , and specifying the transition distribution $p(\hat{\Sigma}_{t_{i+1}} | \hat{\Sigma}_{t_i})$ as

$$\Sigma_{t_{i+1}} \sim p(\Sigma_{t_{i+1}} | \Sigma_{t_i}, \theta_{t_i}), \quad \theta_{t_{i+1}} = \theta_{t_i}.$$

For the augmented latent space $\hat{\Sigma}_{t_i} = (\Sigma_{t_i}, \theta_{t_i})^\top$, we define the observation process as

$$p(y_{t_i} | \hat{\Sigma}_{t_i}) = p(y_{t_i} | \Sigma_{t_i}, \theta_{t_i}) = \mathcal{N}(Hx_{t_i}(\theta_{t_i}), \Gamma + V_{t_i}),$$

as given in (14). By applying a particle filter to the augmented state-space model illustrated in Figure 3, we can sample from the posterior distribution $p(\theta_{t_N}, \Sigma_{t_0}, \dots, \Sigma_{t_N} | y_{t_0}, \dots, y_{t_N})$. Since θ_{t_i} follows a constant transition, the sequence $(\theta_{t_N}, \Sigma_{t_0}, \dots, \Sigma_{t_N})$ of latent variables in the augmented state-space model (Figure 3) follows the original prior distribution $p(\theta, \Sigma_{t_0}, \dots, \Sigma_{t_N})$:

$$(\theta_{t_N}, \Sigma_{t_0}, \dots, \Sigma_{t_N}) \sim p(\theta_{t_N}, \Sigma_{t_0}, \dots, \Sigma_{t_N}) = p(\theta_{t_0}, \Sigma_{t_0}, \dots, \Sigma_{t_N}) = p(\theta, \Sigma_{t_0}, \dots, \Sigma_{t_N}).$$

Correspondingly, the resulting posterior distribution $p(\theta_{t_N}, \Sigma_{t_0}, \dots, \Sigma_{t_N} | y_{t_0}, \dots, y_{t_N})$ is identical to our target posterior $p(\theta, \Sigma_{t_0}, \dots, \Sigma_{t_N} | y_{t_0}, \dots, y_{t_N})$.

4 Markov Prior on Discretization Error Variances

It remains to construct an appropriate Markov prior for the discretization error variances. There are various possible constructions depending on the problem setting, such as the type of ODEs, the numerical method employed, and the available observations. In this section, we review the local propagation of the global error and, based on this analysis, propose a suitable prior.

4.1 Local Propagation of the Global Error

Here, we briefly review the standard theory of error analysis. We distinguish between the *local error* and the *global error*, and discuss the propagation of the latter.

In this subsection, we omit θ for simplicity. We also make the following assumptions:

- The observation time interval is constant, i.e. $t_{i+1} - t_i = \text{const}$.
- The step size used in the time integrator is denoted by h , and $t_{i+1} - t_i = kh$ for a positive integer k .

The first assumption is introduced solely for clarity of presentation. If the second assumption does not hold in practical applications, the solution at $t = t_i$ can be approximated, for example, by interpolation techniques using neighboring numerical solutions [Hairer et al., 1993].

The numerical solution at $t = t_i + jh$ is denoted by $x_{i,j}$ so that $x_{i+1} = x_{i,k}$. The time- h flow for the ODE is denoted by ϕ_h , and the time- h flow of the numerical solver by ψ_h . The local error is defined as the numerical error induced in a single time step, i.e. $\psi_h(x) - \phi_h(x)$. We define

$$L(t_{i,j}) := \psi_h(x_{i,j}) - \phi_h(x_{i,j}) = x_{i,j+1} - \phi_h(x_{i,j}).$$

On the other hand, the global error is defined by

$$G(t_{i,j}) = x_{i,j} - x(t_i + jh).$$

We now examine how the global error propagates. Observe that

$$\begin{aligned} G(t_{i,j+1}) &= x_{i,j+1} - x(t_i + (j+1)h) = \phi_h(x_{i,j}) - \phi_h(x(t_i + jh)) + x_{i,j+1} - \phi_h(x_{i,j}) \\ &= \phi_h(x_{i,j}) - \phi_h(x(t_i + jh)) + L(t_{i,j}). \end{aligned}$$

To analyze the difference $\phi_h(x_{i,j}) - \phi_h(x(t_i + jh))$, we consider the variational equation

$$\frac{d\delta(t)}{dt} = (\nabla_x f(x(t)))\delta(t), \quad \delta(0) = x_{i,j} - x(t_i + jh).$$

For the solution to this equation, it follows that

$$\phi_h(x_{i,j}) - \phi_h(x(t_i + jh)) = \delta(h).$$

By expanding $\delta(h)$ in a Taylor series, we obtain an approximation

$$\delta(h) \approx \delta(0) + h(\nabla_x f(x_{i,j}))\delta(0).$$

Hence, the propagation of the global error satisfies

$$G(t_{i,j+1}) = (I + h\nabla_x f(x_{i,j}) + \mathcal{O}(h^2))G(t_{i,j}) + L(t_{i,j}). \quad (15)$$

4.2 A Markov Prior

Constructing a suitable Markov prior for discretization error variances is crucial. Note that the prior introduced in the previous study [Miyatake et al., 2025] does not satisfy the Markov property and is therefore not appropriate for our setting. In this section, we propose a new Markov prior, motivated by the preceding subsection.

Throughout, we assume that the discretization error variance is diagonal and takes the form

$$\Sigma_{t_i} = \text{diag}\left((\sigma_{t_i}^1)^2, \dots, (\sigma_{t_i}^{d_x})^2\right), \quad (16)$$

and define the vector

$$\sigma_{t_{i+1}} := (\sigma_{t_{i+1}}^1, \dots, \sigma_{t_{i+1}}^{d_x})^\top \in \mathbb{R}_{>0}^{d_x}. \quad (17)$$

We also use the notation $\Sigma_{t_{i,j}}$ and $\sigma_{t_{i,j}}$ with their obvious meanings.

Note that the discretization error variances $\sigma_{t_{i,j}}$ in our context can be interpreted as a model for the global error $G(t_{i,j})$. By identifying $G(t_{i,j})$ in (15) with $\sigma_{t_{i,j}}$, we arrive at the following Markov prior, in which the discretization error variance $\sigma_{t_{i,j}}$ evolves according to the probabilistic transition below as time advances by h :

$$\sigma_{t_{i,j+1}} = M_{i,j} \cdot \sigma_{t_{i,j}} + |\tilde{L}(t_{i,j})|, \quad M_{i,j} \sim P, \quad (j = 0, \dots, k-1). \quad (18)$$

Here, P denotes a distribution over matrices $M_{i,j} \in \mathbb{R}_{>0}^{d_x \times d_x}$. Each component of $M_{i,j}$ is constrained to be nonnegative. The value of $\tilde{L}(t_{i,j})$ is an approximated value of $L(t_{i,j})$. This can be typically estimated by, for example, either $\tilde{L}(t_{i,j}) = \psi_h(x_{i,j}) - \psi_{h/2}(x_{i,j})$ or $\tilde{L}(t_{i,j}) = \psi_h(x_{i,j}) - \tilde{\psi}_h(x_{i,j})$, where $\tilde{\psi}_h$ denotes a higher order numerical solver. These techniques are commonly used to control the step size during time integration [Hairer et al., 1993]. The absolute value $|\cdot|$ of $L(t_{i,j})$ is taken componentwise to ensure consistency with (17), which was defined to be nonnegative.

The proposed Markov prior involves a distribution $M \sim P_\lambda$, which typically depends on a hyperparameter λ . In our experiment, for instance, we set P as $m \cdot I$, where m is drawn from a Gamma distribution $m \sim \text{Gamma}(\alpha, \beta)$; in this case, the hyperparameter $\lambda = (\alpha, \beta)$ must be properly chosen. In the context of particle filtering, this hyperparameter can be tuned by using an empirical Bayes approach, where the marginal likelihood $p(y^*(t_{0:N}) \mid \lambda)$ is estimated via particle methods [Doucet et al., 2001, Kitagawa, 1996].

As shown in the next section, the empirically optimal parameters often satisfy the mean condition

$\mathbb{E}_{M \sim P_\lambda}[M] \approx I$, where I denotes the identity matrix. This observation suggests that it suffices to restrict attention to hyperparameter candidates λ such that $\mathbb{E}_{M \sim P_\lambda}[M] = I$. In the next subsection, we examine this empirical finding from a theoretical perspective.

Remark 3. We have introduced the matrix $M_{i,j}$ in (18) expecting that it plays a similar role to the term $(I + h\nabla_x f(x_{i,j}) + \mathcal{O}(h^2))$ in (15). In this viewpoint, assuming the non-negativity does not pose a problem. Moreover, under some smoothness conditions on f , it follows that $(I + h\nabla_x f(x_{i,j}) + \mathcal{O}(h^2)) \rightarrow I$ as $h \rightarrow +0$, which supports empirical finding mentioned above.

However, taking the absolute value $|\tilde{L}(t_{i,j})|$ of the estimated local error may lead to overestimation. In view of this issue, there is potential to develop a more appropriate model or prior. Nonetheless, we emphasize that the current approach remains effective in many situations, due to the following:

- as shown in the next subsection, the prior satisfies a desirable asymptotic property;
- in phases where the global error increases, adding a positive value appears natural;
- while there might be phases during which the absolute value of the global error decreases (when evaluated componentwise), such phenomena can be captured in the corresponding posterior distribution.

4.3 Asymptotics of the Prior

We investigate asymptotic properties of the proposed prior (18) as the step size h approaches zero. For simplicity in the theoretical analysis, we identify $\tilde{L}(t_{i,j})$ with the exact local error $L(t_{i,j})$, although in practice we estimate it using two numerical solvers. To explicitly show the step-size dependence of the proposed prior, we write the prior as

$$p_h(\sigma_{t_{0,0}}, \dots, \sigma_{t_{N,0}}) = p_h(\sigma_{t_0}, \dots, \sigma_{t_N}) = p_h(\sigma_{t_0}) \cdot \prod_{i=0}^{N-1} p_h(\sigma_{t_{i+1}} | \sigma_{t_i}). \quad (19)$$

Numerical solvers are typically designed so that the numerical error vanishes asymptotically as the step size $h \rightarrow +0$. Accordingly, the proposed prior $p_h(\sigma_{t_i})$ should be defined so that $\sigma_{t_i} \rightarrow 0$ as $h \rightarrow +0$ in the sense of probabilistic convergence. This asymptotic property can be guaranteed by the following theorem, which also provides the corresponding convergence rate:

Theorem 4.1 (Convergence rate in the step-size limit). *Assume that the following conditions (I) ~ (III) hold:*

- (I) A distribution P on matrices M satisfies $\mathbb{E}_{M \sim P}[\|I - M\|_F^2] \leq Lh^2$ for some constant $L > 0$.
- (II) $L(t_{i,j}) = \mathcal{O}(h^{\alpha+1})$ for $0 \leq i \leq N - 1$ and $0 \leq j \leq k - 1$.
- (III) A prior $p_h(\sigma_{t_0})$ on initial time t_0 satisfies $\mathbb{E}_{p_h(\sigma_{t_0})}[\|\sigma_{t_0}\|^2] = \mathcal{O}(h^{2\beta})$ for $\beta \geq 0$.

Then, for $i \geq 1$, we have

$$\sigma_{t_i} = \mathcal{O}_p(h^{\min(\alpha, \beta)}) \quad (h \rightarrow +0). \quad (20)$$

Condition (I) requires that the distribution P be constructed such that $\mathbb{E}_{M \sim P}[\|I - M\|_F^2] = \mathcal{O}(h^2)$. This condition can be easily satisfied by defining a distribution P for which an analytical expression of $\mathbb{E}_{M \sim P}[\|I - M\|_F^2]$ is available, including the one used in our experiments. This condition also requires that P should converge to a Dirac measure at I in the limit $h \rightarrow +0$, which is consistent with Remark 3. Condition (II) defines a given numerical method to be of order α . Condition (III) indicates that the choice of β in the proposed prior at t_1 affects the convergence rate: the prior achieves $\mathcal{O}_p(h^\alpha)$ if $\beta < \alpha$, and $\mathcal{O}_p(h^\beta)$ otherwise.

This theorem shows that the proposed prior is likely to converge in probability at the same rate as the global error $G(t_{i,j}) = x_{t_{i,j}} - x(t_{i,j})$. It is well known that, for many numerical methods, if the local error $L(t_{i,j}) = \mathcal{O}(h^{\alpha+1})$, then the global error $G(t_{i,j})$ is $\mathcal{O}(h^\alpha)$ [Butcher, 2016, Hairer et al., 1993, Iserles, 2008]. Since the discretization error variance in this study corresponds to the global error, the proposed prior is desired to be $\mathcal{O}_p(h^\alpha)$, in order to incorporate this numerical insight into the prior. This theorem shows that the objective is achieved by designing P to satisfy condition (I) and by setting the initial distribution $p_h(\sigma_{t_0})$ such that $\mathbb{E}_{p_h(\sigma_{t_0})}[\|\sigma_{t_0}\|^2] = \mathcal{O}(2^\beta)$ with $\beta \geq \alpha$.

5 Experiments

We evaluate the performance of the proposed method using two examples: the pendulum system and the FitzHugh–Nagumo model. These are representative cases where coarse numerical integration, combined with parameter values that deviate significantly from the true ones, can coincidentally produce trajectories that closely match the observations or the exact solution (obtained using the true parameters).

For both cases, we employ the explicit Euler method as our numerical solver, and also use Runge’s method (the explicit trapezoidal rule) to estimate the local discretization errors. The explicit Euler method is chosen to represent a scenario in which discretization errors may be significant. The observations are generated by adding randomly sampled noise to the reference solution, which is computed using a sufficiently accurate solver. The reference solution is also used to calculate the *exact* discretization errors. All numerical experiments were implemented in `Julia`.

5.1 Pendulum System

We consider the pendulum system $y''(t) = (-g/L) \sin y(t)$, where $g := 9.81$ denotes the gravitational acceleration. This system involves a parameter $\theta = L$ that is to be inferred from observations. The system is equivalent to the first-order system

$$\frac{d}{dt} \begin{bmatrix} y_1(t) \\ y_2(t) \end{bmatrix} = \begin{bmatrix} y_2(t) \\ -\frac{g}{L} \sin y_1(t) \end{bmatrix}. \quad (21)$$

We employ the explicit Euler method with step size $h = 0.05$. The observation operator H is set to $\text{diag}(3.0, 3.0)$.

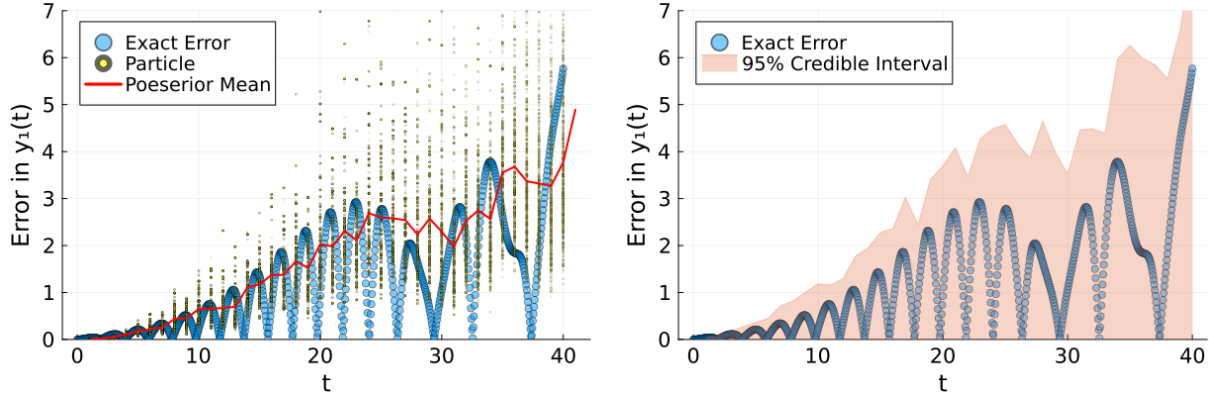


Figure 4: Discretization error quantification results for $y_1(t)$ in the pendulum system. **Left:** the first component $\sigma_{t_i}^1$ of the particle $\sigma_{t_i} = (\sigma_{t_i}^1, \sigma_{t_i}^2)^\top$. **Right:** the 95% credible interval evaluated using samples $r_{t_i}^1 \sim \mathcal{N}(0, (\sigma_{t_i}^1)^2)$ drawn from the posterior predictive distribution.

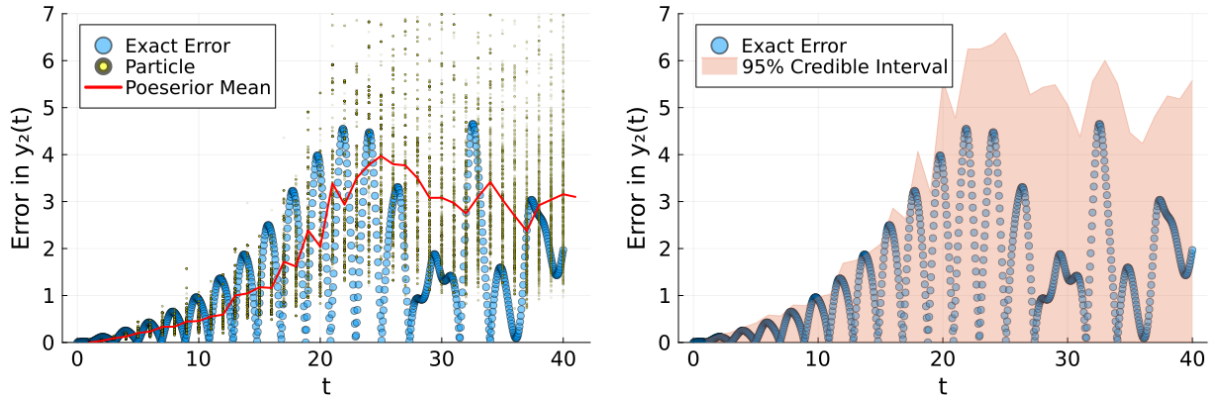


Figure 5: Discretization error quantification results for $y_2(t)$ in the pendulum system. **Left:** the second component $\sigma_{t_i}^2$ of the particle $\sigma_{t_i} = (\sigma_{t_i}^1, \sigma_{t_i}^2)^\top$. **Right:** the 95% credible interval evaluated using samples $r_{t_i}^2 \sim \mathcal{N}(0, (\sigma_{t_i}^2)^2)$ drawn from the posterior predictive distribution.

5.1.1 Discretization Error Quantification

We first assess the performance of the proposed method (described in Section 3.1) with the parameter L fixed at $L^* = 3.0$. Observations are given at $t = 1, 2, \dots, 40$ with the covariance matrix given by $\Gamma = \text{diag}(1.0^2, 1.0^2)$. The number of particles is set to 1000, and the distribution P is fixed to $m \cdot I$ with $m \sim \text{Gam}(\alpha, \beta)$. The hyperparameters (α, β) are selected from the candidate sets $\alpha \in \{50.0, 55, 60, \dots, 800.0\}$ and $\beta \in \{0.001, 0.00125, 0.0015, \dots, 0.033\}$, yielding a total of $151 \cdot 129 = 19,479$ candidates.

Figures 4 and 5 show the discretization error quantification results for $y_1(t)$ and $y_2(t)$ in (21), respectively. For both cases, the absolute values of the exact discretization errors are plotted (“Exact Error” in the figures). The left panels of Figures 4 and 5 present the first component $\sigma_{t_i}^1$ and the second component $\sigma_{t_i}^2$ of the particles $\sigma_{t_i} = (\sigma_{t_i}^1, \sigma_{t_i}^2)^\top$ obtained by the proposed method. Recalling that the discretization error variance Σ_{t_i} for $(y_1(t), y_2(t))^\top$ is expressed as $\text{diag}((\sigma_{t_i}^1)^2, (\sigma_{t_i}^2)^2)$ as discussed in (16), $(\sigma_{t_i}^1)^2$ and $(\sigma_{t_i}^2)^2$ correspond to the discretization error variances for $y_1(t)$ and $y_2(t)$, respectively. We observe that the particles successfully capture the temporal trend of the exact errors. In particular, the decrease in

Rank	(α, β)	$\alpha \cdot \beta$	Log-likelihood
1	(335.000, 0.0030)	1.0050	-241.806424
2	(365.000, 0.0027)	1.0037	-242.531858
3	(670.000, 0.0015)	1.0050	-243.266446
4	(155.000, 0.0065)	1.0075	-243.994101
5	(175.000, 0.0057)	1.0063	-244.423485
6	(445.000, 0.0022)	1.0012	-245.456227
7	(130.000, 0.0077)	1.0075	-245.996058
8	(575.000, 0.0018)	1.0063	-246.007687
9	(310.000, 0.0032)	1.0075	-246.112785
10	(115.000, 0.0088)	1.0063	-246.484862

Table 1: Top 10 parameter pairs (α, β) with their corresponding log-likelihood values $\log p(y_{1:40}^* | \alpha, \beta)$ in the experiment for the pendulum system.

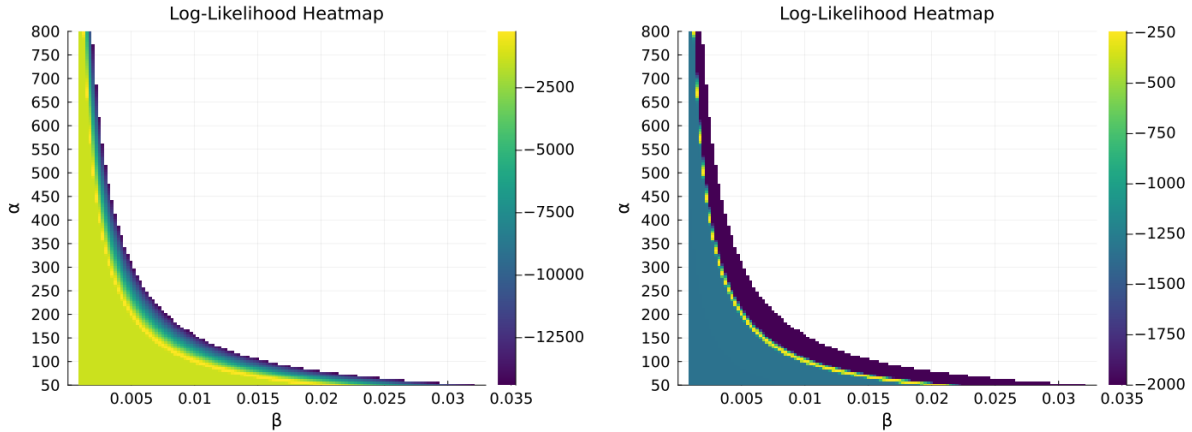


Figure 6: Log-likelihood heatmaps in the pendulum system. White regions indicate that the likelihood is effectively zero (i.e., output of the log-likelihood is $-\text{Inf}$). Left: heatmap over all candidate hyperparameter settings. Right: heatmap with the color scale fixed below -2000 to emphasize higher-likelihood regions.

the exact errors around $t = 30$ is accurately reflected via the proposed method. Such behavior cannot be captured by previous approaches [Marumo et al., 2024, Matsuda and Miyatake, 2021, Miyatake et al., 2025], which assume that the discretization error increases monotonically. Figures 4 and 5 also depict the 95% credible interval of the discretization errors, drawn from the posterior predictive distribution. Specifically, each $r_{t_i}^1$ and $r_{t_i}^2$ is sampled from normal distributions $\mathcal{N}(0, (\sigma_{t_i}^1)^2)$ and $\mathcal{N}(0, (\sigma_{t_i}^2)^2)$, where each variance parameter σ_{t_i} is randomly selected from the set of particles obtained by the proposed method. We can confirm that a substantial proportion of the exact discretization errors lie within this credible interval.

We examine the behavior of the hyperparameters (α, β) selected by the empirical Bayesian approach. Note that under our setting, where $M = m \cdot I$ with $m \sim \text{Gam}(\alpha, \beta)$, we have

$$\mathbb{E}_{M \sim P_{(\alpha, \beta)}}[M] = \text{diag}(\mathbb{E}_{m \sim \text{Gam}(\alpha, \beta)}[m], \dots, \mathbb{E}_{m \sim \text{Gam}(\alpha, \beta)}[m]) = \text{diag}(\alpha \cdot \beta, \dots, \alpha \cdot \beta).$$

Table 1 lists the top 10 parameter pairs selected from the 19,749 candidates. We observe that the selected parameters tend to satisfy $\alpha \cdot \beta \approx 1$, which is consistent with the theoretical implications discussed in

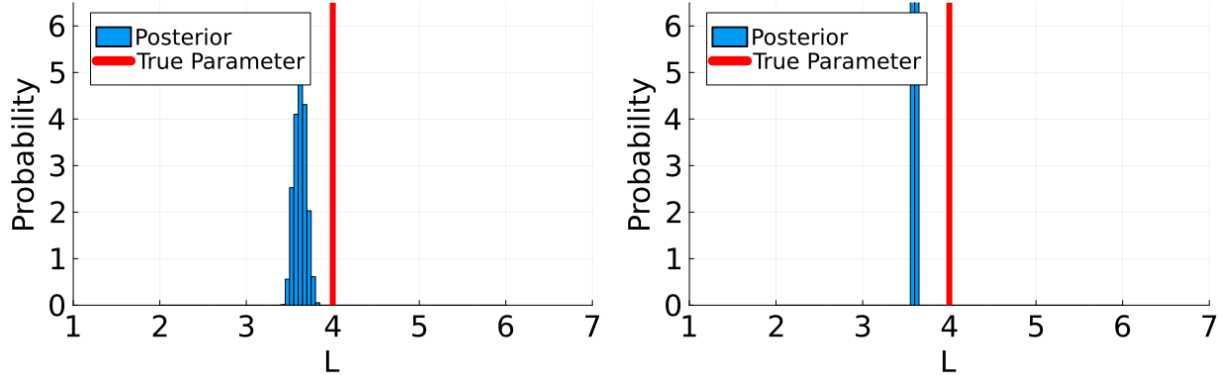


Figure 7: Posterior distributions of the ODE parameter L for the pendulum system. The left panel shows the posterior obtained using Algorithm 2 with the proposed prior on the discretization error variances, whereas the right panel shows the posterior obtained by applying Algorithm 2 with $\sigma_{t_i} = (0, 0)^\top$ for all t_i .

Section 4. Figure 6 shows the heatmap of the log-likelihood for each parameter candidate. We find that regions of low likelihood align with the curve $\alpha \cdot \beta = 1$.

5.1.2 Parameter Inference with Discretization Error Quantification

Next, we assess the performance of the proposed method (described in Section 3.2) that jointly estimate the discretization error variance and the ODE parameter. The observations are generated from the process with the true parameter value $L^* = 4.0$ at discrete time points $t = 11, \dots, 40$, with the covariance matrix set to $\Gamma = \text{diag}(2.0^2, 2.0^2)$. A prior on the ODE parameter L is specified as $\mathcal{N}(3.0, 2.0^2)$. The number of particles is set to 80,000. The hyperparameters (α, β) are chosen from the pair $\lambda = (\alpha, 1/\alpha)$, where $\alpha \in \{5.0, 10.0, 15.0, \dots, 500.0\}$.

Figure 7 shows the posterior distributions of the ODE parameter, comparing it with an alternative that does not account for discretization errors. The latter is obtained by implementing Algorithm 2, with $\sigma_{t_i} = (0.0, 0.0)^\top$ for all t_i . As observed in the figure, the peaks of both posteriors are slightly shifted to the left of the true parameter $L^* = 4.0$. However, the proposed method exhibits broader support, as it accounts for discretization errors. In contrast, the posterior that ignores discretization errors behaves like a direct measure, indicating that such neglect leads to highly confident yet inaccurate parameter estimates.

Figures 8 and 9 show discretization error quantification results for $y_1(t)$ and $y_2(t)$ respectively. These results show that the proposed method underestimates the discretization error. This is likely due to the fact that, in the presence of discretization errors, some particles become concentrated around parameter values different from $L^* = 4.0$ that happen to match the observations. As a result, the method may incorrectly infer that the discretization error is small, highlighting a potential limitation of the proposed approach.

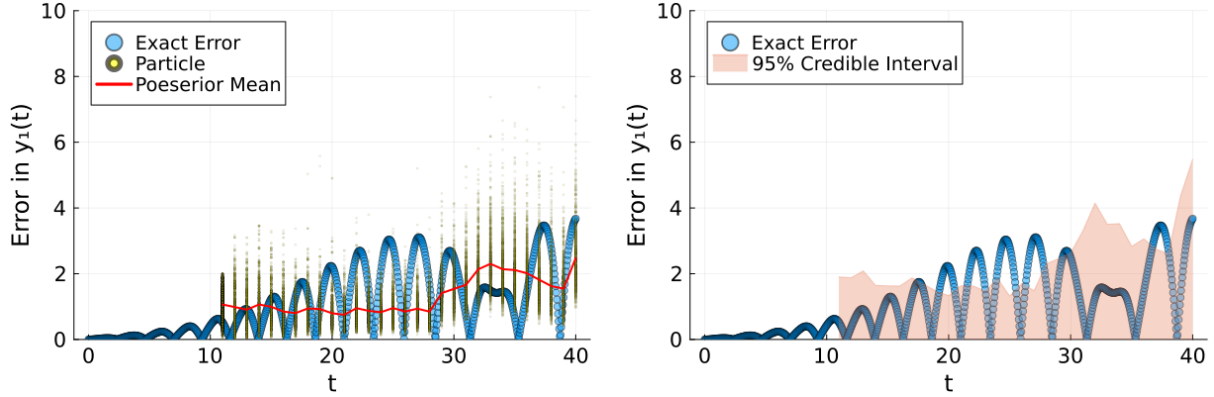


Figure 8: Discretization error quantification results for $y_1(t)$ in the pendulum system. **Left:** the first component $\sigma_{t_i}^1$ of the particle $\sigma_{t_i} = (\sigma_{t_i}^1, \sigma_{t_i}^2)^\top$. **Right:** the 95% credible interval evaluated using samples $r_{t_i}^1 \sim \mathcal{N}(0, (\sigma_{t_i}^1)^2)$ drawn from the posterior predictive distribution.

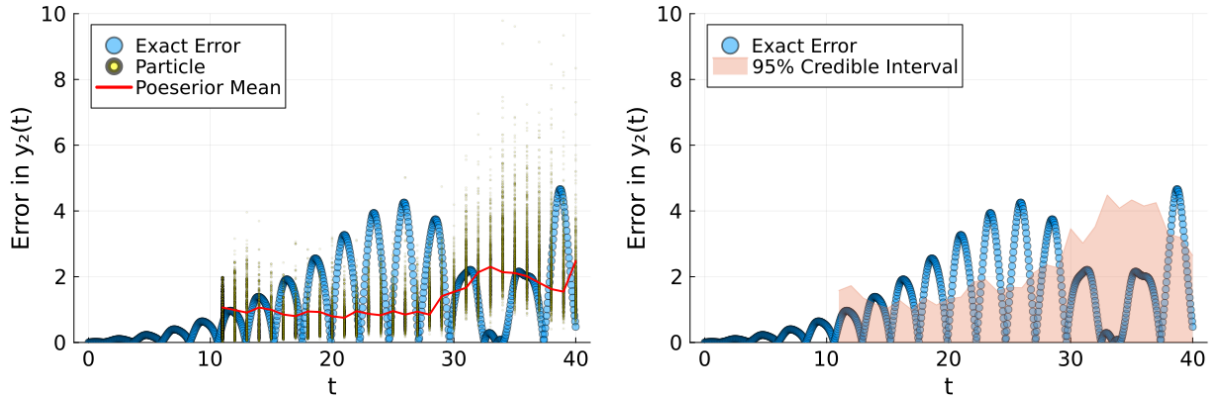


Figure 9: Discretization error quantification results for $y_2(t)$ in the pendulum system. **Left:** the second component $\sigma_{t_i}^2$ of the particle $\sigma_{t_i} = (\sigma_{t_i}^1, \sigma_{t_i}^2)^\top$. **Right:** the 95% credible interval evaluated using samples $r_{t_i}^2 \sim \mathcal{N}(0, (\sigma_{t_i}^2)^2)$ drawn from the posterior predictive distribution.

5.2 FitzHugh–Nagumo model

We also demonstrate the effectiveness of the proposed method with the FitzHugh–Nagumo (FN) model:

$$\frac{d}{dt} \begin{bmatrix} V \\ R \end{bmatrix} = \begin{bmatrix} c \left(V - \frac{V^3}{3} + R \right) \\ -\frac{1}{c} (V - a + bR) \end{bmatrix}. \quad (22)$$

The two-dimensional differential equation involves three unknown parameters, $\theta = (a, b, c)$, which are to be inferred. We employ the explicit Euler method with a step size of $h = 0.2$. The observation operator H is set to the identity matrix.

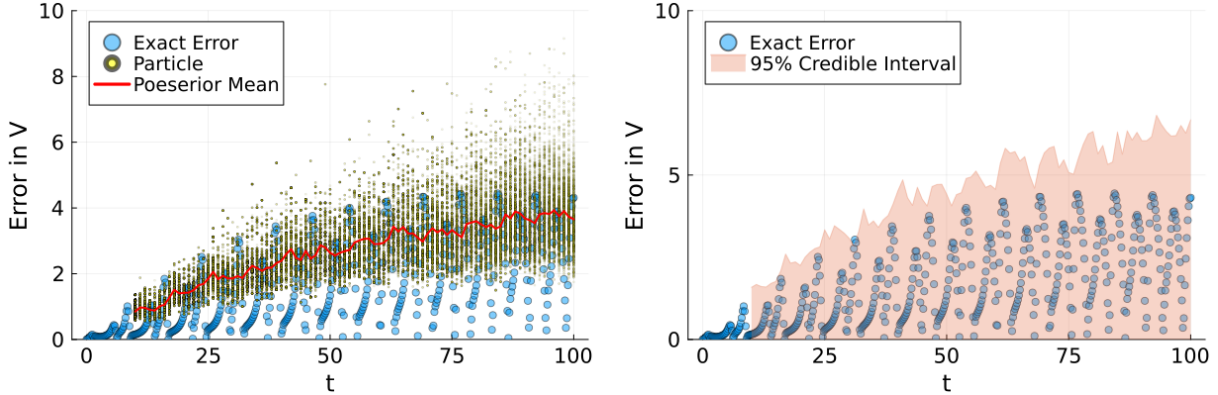


Figure 10: Discretization error quantification results for V in the FitzHugh–Nagumo model. **Left:** the first component $\sigma_{t_i}^1$ of the particle $\sigma_{t_i} = (\sigma_{t_i}^1, \sigma_{t_i}^2)^\top$. **Right:** the 95% credible interval evaluated using samples $r_{t_i}^1 \sim \mathcal{N}(0, (\sigma_{t_i}^1)^2)$ drawn from the posterior predictive distribution.

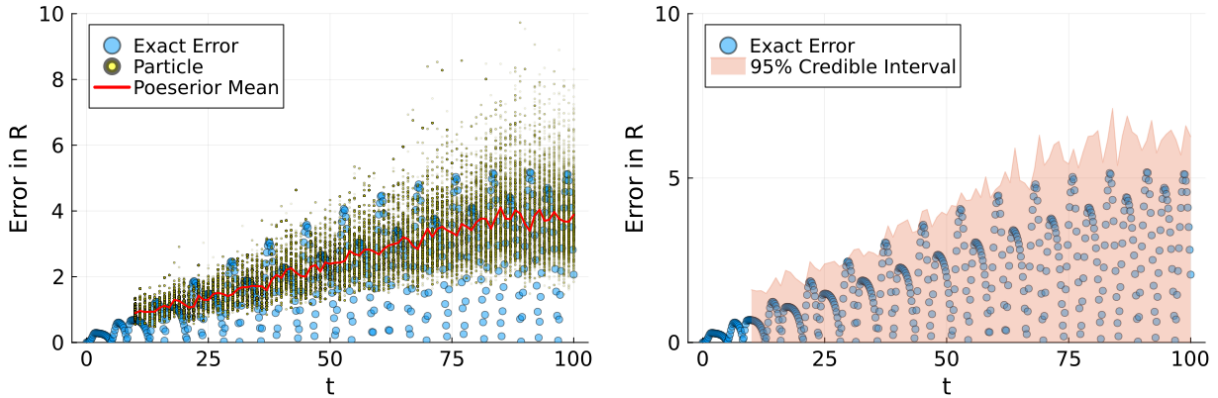


Figure 11: Discretization error quantification results for R in the FitzHugh–Nagumo model. **Left:** the second component $\sigma_{t_i}^2$ of the particle $\sigma_{t_i} = (\sigma_{t_i}^1, \sigma_{t_i}^2)^\top$. **Right:** the 95% credible interval evaluated using samples $r_{t_i}^2 \sim \mathcal{N}(0, (\sigma_{t_i}^2)^2)$ drawn from the posterior predictive distribution.

5.2.1 Discretization Error Quantification

We assess the performance of the proposed method (described in Section 3.1) with the parameters fixed at $(a^*, b^*, c^*) = (0.2, 0.1, -0.5)$. The covariance matrix of the observation noise is set to $\Gamma = \text{diag}(0.1^2, 0.1^2)$. Observation data $y_{t_i}^*$ are obtained at 91 discrete time points, $t_i = 10, 11, \dots, 100$. The number of particles is set to 1,000, and the distribution P is fixed to $m \cdot I$ with $m \sim \text{Gam}(\alpha, \beta)$. The hyperparameters (α, β) are selected from the candidate sets $\alpha \in \{5.0, 10.0, \dots, 500.0\}$ and $\beta \in \{0.002, 0.004, \dots, 1.0\}$, yielding a total of $100 \cdot 500 = 50,000$ candidates. We evaluate the log-likelihoods $\log p(y_{10:100}^* | \alpha, \beta)$ for (α, β) using 50 particles, and choose the pair that achieves the maximum log-likelihood.

Figures 10 and 11 show discretization error quantification results for V and R in the FN model, along with the absolute values of the exact discretization errors r_i . We can confirm that the temporal evolution of the particles and the 95% credible intervals closely follows the time course of the discretization error r_i , demonstrating the effectiveness of the proposed approach.

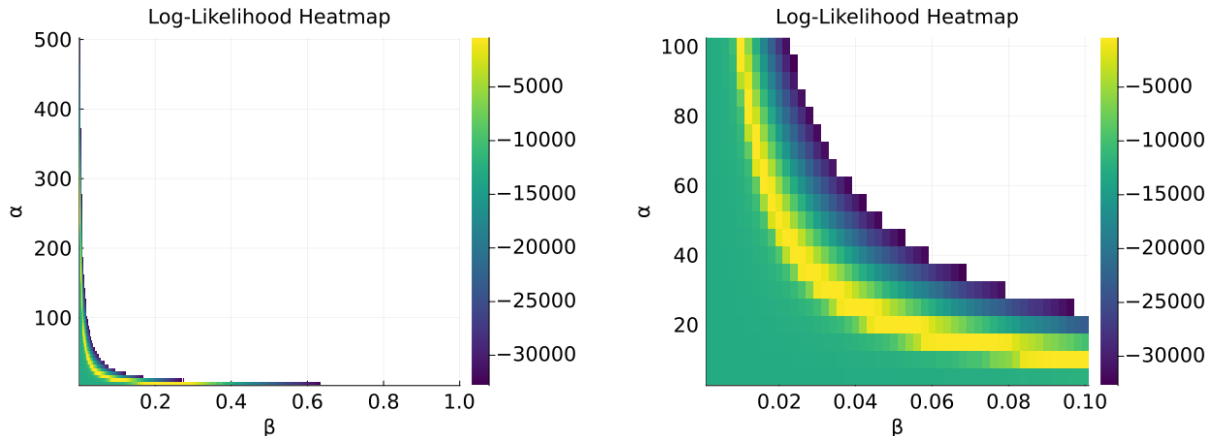


Figure 12: Log-likelihood heatmaps in Subsection 5.2.1. White regions indicate that the likelihood is effectively zero (i.e., output of the log-likelihood is $-\text{Inf}$). Left: full hyperparameter range. Right: zoomed region with $\alpha \in \{5, \dots, 100\}$ and $\beta \in \{0.002, 0.004, \dots, 0.10\}$.

Figure 12 presents a heatmap of the log-likelihoods $\log p(y_{10:100}^* | \alpha, \beta)$ for all candidate parameter pairs. The heatmap indicates that parameter pairs with low log-likelihood values tend to cluster along the curve defined by $\alpha \cdot \beta = 1$, similar to what is observed for the pendulum system.

5.2.2 Parameter Inference with Discretization Error Quantification

We address the simultaneous inference of ODE parameters and discretization errors using the self-organizing technique described in Subsection 3.2. The priors for the ODE parameters are set as follows:

$$a \sim \mathcal{N}_{[-1.5, 1.5]}(0, 0.9^2), \quad b \sim \mathcal{N}_{[-0.1, 1.0]}(1.0, 1.0^2), \quad c \sim \mathcal{N}_{[0.1, 2.0]}(1.0, 1.0^2),$$

where $\mathcal{N}_{[s_1, s_2]}(\mu, \sigma^2)$ denotes a truncated normal distribution of $\mathcal{N}(\mu, \sigma^2)$ restricted to the interval $[s_1, s_2]$. The number of particles is fixed at 500,000, which is larger than in the previous subsection to account for the increased dimensionality of the latent space. The noise matrix Γ in the observation process is set to $\text{diag}(1.0^2, 1.0^2)$. Observations $y_{t_i}^*$ are assumed to be obtained at time points $t_i = 10, 11, \dots, 50$, with the true parameter fixed at $(a^*, b^*, c^*) = (0.5, 0.2, 1.0)$. The distribution P_λ is $m \cdot I \sim P_\lambda$, where $m \sim \text{Gam}(\alpha, \beta)$, as in the previous sections. The hyperparameters (α, β) are selected from the pair $\lambda = (\alpha, \frac{1}{\alpha})$, such that $\alpha \cdot \frac{1}{\alpha} = 1$, where $\alpha \in \{2.0, 4.0, 6.0, \dots, 50.0\}$.

Figures 13 and 14 show discretization error quantification results. It can be seen that the discretization error in V is overestimated, particularly around time $t = 20$. This overestimation is likely due to the local error $L(t_i)$ also being overestimated in the interval $t = 20 \sim 30$. After $t = 30$, the particles are more widely spread; however, on average, they are located close to the exact error. Regarding the discretization error variance in R , we can see that the proposed method successfully captures the exact discretization errors.

Figure 15 presents the posterior distributions of the ODE parameters obtained using the proposed method, compared with those obtained by ignoring discretization errors. The latter is computed in the

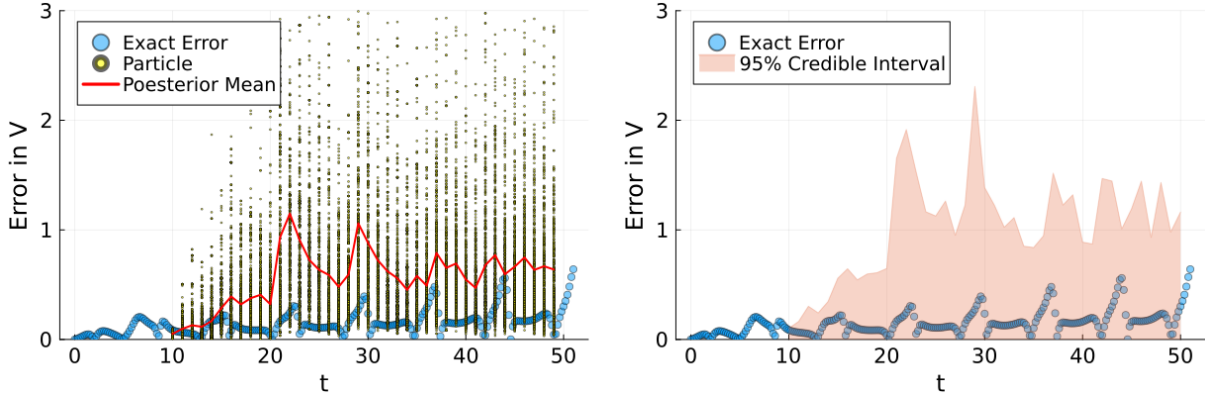


Figure 13: Discretization error quantification results for V in the FitzHugh–Nagumo model. **Left:** the first component $\sigma_{t_i}^1$ of the particle $\sigma_{t_i} = (\sigma_{t_i}^1, \sigma_{t_i}^2)^\top$. **Right:** the 95% credible interval evaluated using samples $r_{t_i}^1 \sim \mathcal{N}(0, (\sigma_{t_i}^1)^2)$ drawn from the posterior predictive distribution.

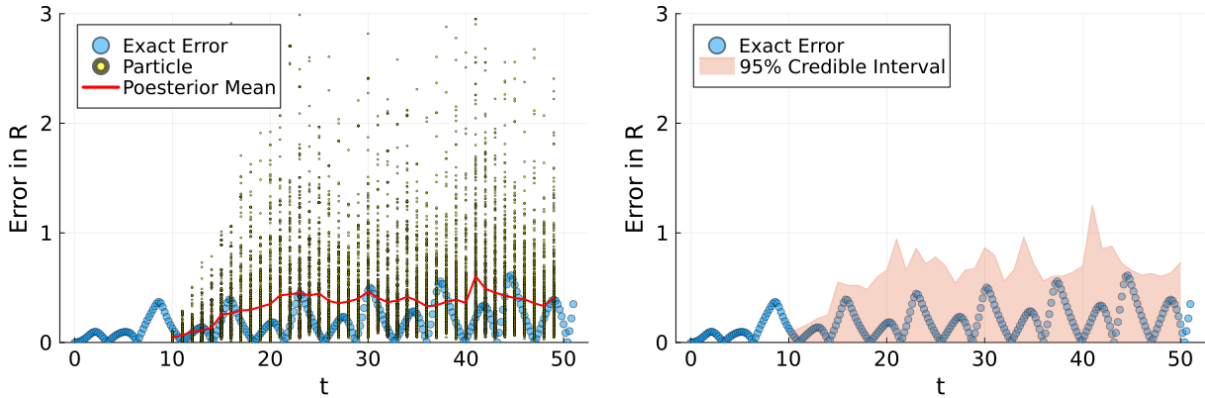


Figure 14: Discretization error quantification results for R in the FitzHugh–Nagumo model. **Left:** the second component $\sigma_{t_i}^2$ of the particle $\sigma_{t_i} = (\sigma_{t_i}^1, \sigma_{t_i}^2)^\top$. **Right:** the 95% credible interval evaluated using samples $r_{t_i}^2 \sim \mathcal{N}(0, (\sigma_{t_i}^2)^2)$ drawn from the posterior predictive distribution.

same manner as in the pendulum system. The results show that ignoring discretization errors yields posterior distributions that fail to capture the true parameters, particularly a and c . In contrast, when the discretization error variances are taken into account, the supports of the posterior distributions shift toward the true parameter values.

6 Conclusion

In this study, we proposed a Bayesian framework for parameter estimation in ordinary differential equation (ODE) models that explicitly accounts for discretization errors introduced by numerical solvers. Our approach models these discretization errors as random variables and performs joint Bayesian inference on both the ODE parameters and the corresponding discretization error variances. By imposing a Markov property on a prior over the discretization error variances, we reformulate the inference problem into a state-space modeling framework. We also proposed a Markov prior motivated by a fundamental principle from numerical analysis: global discretization errors accumulate from local errors. We established a

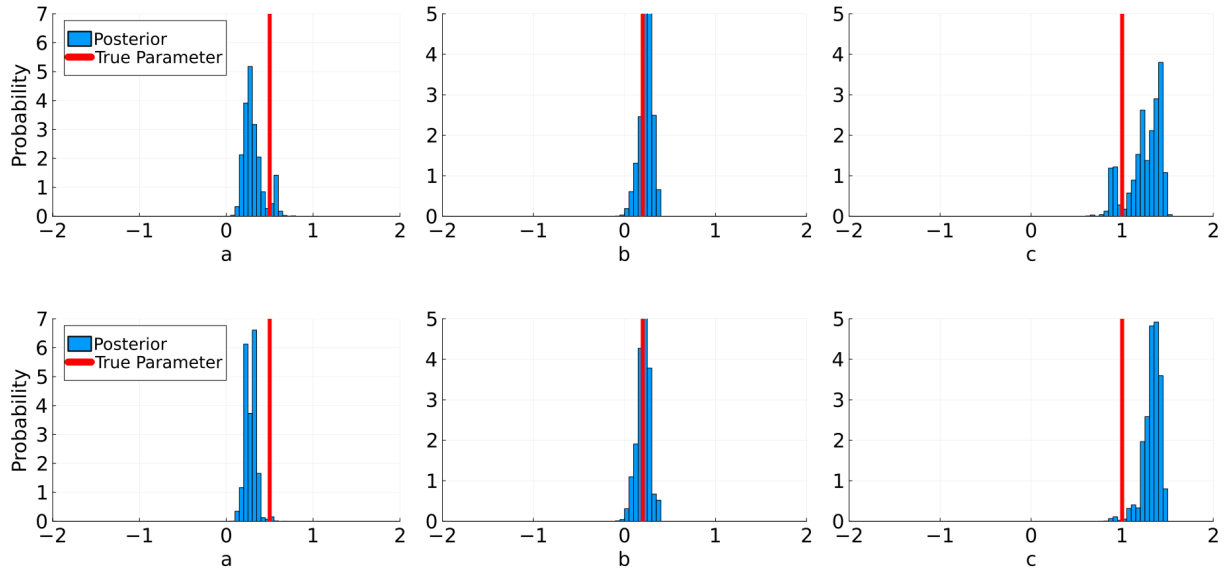


Figure 15: Posterior distributions of the ODE parameters (a, b, c) for the FitzHugh-Nagumo model. The first row shows the posterior obtained using Algorithm 2 with the proposed prior on the discretization error variances, whereas the second row shows the posterior obtained by applying Algorithm 2 with $\sigma_{t_i} = (0, 0)^T$ for all t_i .

convergence rate for the proposed prior as the solver step size tends to zero, thereby providing a theoretical guarantee. The effectiveness of the proposed approach is demonstrated through numerical experiments on the pendulum system and the FitzHugh–Nagumo model, showing improved parameter estimation and uncertainty quantification.

Several directions remain for future work. First, the proposed prior assumes that the discretization error variances are diagonal, which limits its ability to capture correlations among the discretization errors. Developing an appropriate Markov prior for the non-diagonal case—based, for instance, on the Wishart distribution—remains an important open problem.

Another promising direction is to extend the proposed method to high-dimensional systems, including semi-discretized systems for partial differential equations. Although particle filters are attractive due to their minimal modeling assumptions, they often fail to scale effectively in high-dimensional settings. In contrast, extended and ensemble Kalman filters are generally better suited to such scenarios but require assumptions, such as linearity and Gaussianity. Designing a prior that satisfies these assumptions is therefore an important avenue for future research.

Finally, integrating the proposed framework with the field of simulation-based inference (SBI) offers another compelling direction. SBI has emerged as a powerful approach for parameter inference through model simulations [Cranmer et al., 2020]. In particular, recent advances in deep neural network–based methods have greatly expanded its applicability to high-dimensional simulators [Papamakarios and Murray, 2016, Radev et al., 2023, Wildberger et al., 2023] or simulators constructed by differential equations [Gloeckler et al., 2025, Hikida et al., 2025]. However, discretization errors introduced by numerical solvers have not yet been incorporated into SBI methodologies. Developing SBI methodologies that explicitly

account for such errors is an important future challenge.

A Derivation of Smoothing in Particle Filters

In this appendix, we provide the mathematical background for the simultaneous resampling technique (12), used to obtain smoothed particles $\{(\Sigma_{0|0}^k, \dots, \Sigma_{i|0:i}^k)\}_{k=1}^K$ that represent the distribution $p(\Sigma_{0:i} | y_{0:i}^*)$, which plays a central role in the present work. This technique was originally proposed by Kitagawa [Kitagawa, 1996].

We establish the result by mathematical induction. Assume that we already have smoothed particles $\{(\Sigma_{0|0}^k, \dots, \Sigma_{i|0:i}^k)\}_{k=1}^K$ representing the distribution $p(\Sigma_{0:i} | y_{0:i}^*)$. Then, by the prediction step $\Sigma_{i+1|0:i}^k \sim p(\Sigma_{i+1} | \Sigma_{i|0:i}^k)$, we obtain particles $\{(\Sigma_{0|0}^k, \dots, \Sigma_{i|0:i}^k, \Sigma_{i+1|0:i}^k)\}_{k=1}^K$ that approximate the distribution $p(\Sigma_{0:i+1} | y_{0:i}^*)$, one step ahead in time.

From straightforward computation, we have

$$\begin{aligned} p(\Sigma_{0:i+1} | y_{0:i+1}) &= \frac{p(y_{i+1} | \Sigma_{0:i+1}, y_{0:i}) p(\Sigma_{0:i+1} | y_{1:i})}{p(y_{i+1} | y_{0:i})} \\ &\propto p(y_{i+1} | \Sigma_{0:i+1}, y_{1:i}) p(\Sigma_{0:i+1} | y_{0:i}) \\ &= p(y_{i+1} | \Sigma_{i+1}) p(\Sigma_{0:i+1} | y_{0:i}), \end{aligned} \tag{23}$$

where the final equality follows from the hidden Markov structure, that assumes conditional independence between y_{i+1} and $(\Sigma_{0:i}, y_{1:i})$ given Σ_{i+1} .

Recall that we have a particle approximation $\{(\Sigma_{0|0}^k, \dots, \Sigma_{i|0:i}^k, \Sigma_{i+1|0:i}^k)\}_{k=1}^K$ for the distribution $p(\Sigma_{0:i+1} | y_{0:i}^*)$. Substituting this approximation into (23) gives

$$p(\Sigma_{0:i+1} | y_{0:i+1}^*) \propto p(y_{i+1}^* | \Sigma_{i+1}) p(\Sigma_{0:i+1} | y_{0:i}^*) \approx \sum_{k=1}^K w_k \delta_{(\Sigma_{0|0}^k, \dots, \Sigma_{i|0:i}^k, \Sigma_{i+1|0:i}^k)},$$

where the weights w_k are defined as in (10). By applying the same argument as in the correction step of Subsection 3.1, the particles $\{(\Sigma_{0|0}^k, \dots, \Sigma_{i|0:i+1}^k)\}_{k=1}^K$ obtained by the resampling step (12) yield a particle approximation for $p(\Sigma_{0:i+1} | y_{0:i+1}^*)$.

B Proof of Theorem 4.1

In this appendix, we prove Theorem 4.1. While (19) defines the Markov prior only at the observation points t_0, \dots, t_N , the recursive construction in (18) naturally allows us to extend this definition to finer time grids as follows:

$$p_h(\sigma_{t_{0,0}}, \sigma_{t_{0,1}}, \dots, \sigma_{t_{0,k-1}}, \sigma_{t_{1,0}}, \dots, \sigma_{t_{N,0}}) = p_h(\sigma_{t_{0,0}}) \prod_{i=0}^{N-1} \cdot \prod_{j=0}^{k-1} p_h(\sigma_{t_{i,j+1}} | \sigma_{t_{i,j}}).$$

Proof of Theorem 4.1. Let us recall that random variables $\{X_h\}_{h>0}$ and $\{Y_h\}_{h>0}$ indexed by h satisfy

$X_h = \mathcal{O}_p(Y_h)$ if X_h/Y_h is uniformly tight:

$$\lim_{\epsilon \rightarrow \infty} \sup_h \mathbb{P} \left(\left| \frac{X_h}{Y_h} \right| \geq \epsilon \right) = 0.$$

By Chebyshev's inequality [Durrett, 2019, Theorem 1.6.4.], we have

$$\sup_h \mathbb{P} \left(\left| \frac{\sigma_{t_i}}{h^{\min(\alpha, \beta)}} \right| \geq \epsilon \right) \leq \sup_h \frac{1}{\epsilon^2 \cdot h^{2 \min(\alpha, \beta)}} \mathbb{E}_{\sigma_{t_i} \sim p_h(\sigma_{t_i})} [\|\sigma_{t_i}\|^2]. \quad (24)$$

Hence, it suffices to prove that $\mathbb{E}_{p_h(\sigma_{t_i})} [\|\sigma_{t_i}\|^2] = \mathcal{O}(h^{2 \min(\alpha, \beta)})$ for $i \geq 1$.

Define $e_{i,j} := \mathbb{E}_{p_h(\sigma_{t_{i,j}})} [\|\sigma_{t_{i,j}}\|^2]$ to simplify the notation. By the definition (18), it holds that for $0 \leq i \leq (N-1)$ and $0 \leq j \leq k-1$,

$$\sigma_{t_{i,j+1}} = M_{i,j} \cdot \sigma_{t_{i,j}} + |L(t_{i,j})|.$$

This leads to the inequality

$$\begin{aligned} e_{i,j+1} &= \mathbb{E}_{p_h(\sigma_{t_{i,j+1}})} [\|\sigma_{i,j+1}\|^2] \\ &= \mathbb{E}_{p_h(\sigma_{t_{i,j}}), P} [\|M_{i,j} \cdot \sigma_{t_{i,j}} + |L(t_{i,j})|\|^2] \\ &\leq \mathbb{E}_{p_h(\sigma_{t_{i,j}}), P} [\|M_{i,j} \cdot \sigma_{t_{i,j}}\|^2] + \|L(t_{i,j})\|^2 \\ &\leq \mathbb{E}_{p_h(\sigma_{t_{i,j}}), P} [\|M_{i,j}\|_F^2 \cdot \|\sigma_{t_{i,j}}\|^2] + \|L(t_{i,j})\|^2 \\ &\leq \mathbb{E}_P [\|M_{i,j}\|_F^2] \cdot \mathbb{E}_{p_h(\sigma_{t_{i,j}})} [\|\sigma_{t_{i,j}}\|^2] + \|L(t_{i,j})\|^2 \\ &= \mathbb{E}_P [\|I - (I - M_{i,j})\|_F^2] \cdot e_{i,j} + \|L(t_{i,j})\|^2 \\ &\leq \{ \mathbb{E}_P [\|I\|_F^2] + \mathbb{E}_P [\|I - M_{i,j}\|_F^2] \} \cdot e_{i,j} + \|L(t_{i,j})\|^2 \\ &\leq (1 + Lh^2) \cdot e_{i,j} + \|L(t_{i,j})\|^2 \end{aligned} \quad (25)$$

$$\leq (1 + Lh^2) \cdot e_{i,j} + C_{i,j}^2 h^{2\alpha+2} \quad (26)$$

Here, the inequality in (25) follows from Assumption (I), whereas the one in (26) can be obtained by choosing $C_{i,j}$ such that $\|L(t_{i,j})\| \leq C_{i,j} h^{p+1}$. The existence of such constants $C_{i,j}$ is guaranteed by Assumption (III). Setting $C = \max_{0 \leq i \leq N-1, 0 \leq j \leq k-1} C_{i,j}$, we have a uniform bound

$$(26) \leq (1 + Lh^2) \cdot e_{i,j} + C^2 h^{2\alpha+2}, \quad (27)$$

which does not depend on index (i, j) . Applying (27) recursively, we obtain

$$\begin{aligned}
e_{i,j+1} &\leq (1 + Lh^2)^{j+1+ik} \cdot e_{0,0} + C^2 h^{2\alpha+2} \sum_{l=1}^{j+ik+1} (1 + Lh^2)^{l-1} \\
&= (1 + Lh^2)^{j+1+ik} \cdot e_{0,0} + C^2 h^{2\alpha+2} \cdot \frac{(1 + Lh^2)^{j+1+ik} - 1}{Lh^2} \\
&\leq \exp((j+1+ik)Lh^2) \cdot e_{0,0} + C^2 h^{2\alpha} \cdot \frac{\exp((j+1+ik)Lh^2) - 1}{L} \\
&\leq \exp(L((j+1+ik)h)^2) \cdot e_{0,0} + C^2 h^{2\alpha} \cdot \frac{\exp(L((j+1+ik)h)^2) - 1}{L}. \tag{28} \\
&\leq \exp(L(t_{i,j+1} - t_0)^2) \cdot e_{0,0} + C^2 h^{2\alpha} \cdot \frac{\exp(L((t_{i,j+1} - t_0))^2) - 1}{L}. \tag{29}
\end{aligned}$$

Since this equality holds for $j = k - 1$ and $0 \leq i \leq N - 1$, we have

$$\begin{aligned}
\mathbb{E}_{p_h(\sigma_{t_i})}[\|\sigma_{t_i}\|^2] &= \mathbb{E}_{p_h(\sigma_{t_{i-1,k}})}[\|\sigma_{t_{i-1,k}}\|^2] = e_{i-1,k} = e_{i-1,(k-1)+1} \\
&\leq \exp(L(t_{i-1,k} - t_0)^2) \cdot e_{0,0} + C^2 h^{2\alpha} \cdot \frac{\exp(L(t_{i-1,k} - t_0)^2) - 1}{L} \tag{30}
\end{aligned}$$

$$\leq \exp(L(t_i - t_0)^2) \cdot e_{0,0} + C^2 h^{2\alpha} \cdot \frac{\exp(L(t_i - t_0)^2) - 1}{L}. \tag{31}$$

Note that $e_{0,0} = \mathbb{E}_{p_h(\sigma_{t_0})}[\|\sigma_{t_0}\|^2] = \mathcal{O}(h^{2\beta})$ (Assumption (III)), and therefore the first term in (31) is also of order $\mathcal{O}(h^{2\beta})$. This implies that (31) is of order $\mathcal{O}(h^{2\min(\alpha,\beta)})$, which concludes the proof. \square

Acknowledgements

This work is supported by JSPS KAKENHI Grant Numbers 24K02951, 24K00540, 25H00449, 24K20750, JP25H01454 and JST ACT-X, Japan, Grant Number JPMJAX25CH.

References

- Richard FitzHugh. Impulses and physiological states in theoretical models of nerve membrane. *Biophysical journal*, 1(6):445–466, 1961.
- William Ogilvy Kermack and Anderson G McKendrick. A contribution to the mathematical theory of epidemics. *Proceedings of the royal society of london. Series A, Containing papers of a mathematical and physical character*, 115(772):700–721, 1927.
- Vito Volterra. Fluctuations in the abundance of a species considered mathematically. *Nature*, 119:12–13, 1926.
- Katsuhiko Ogata. *Modern control engineering*. Prentice hall, 2010.
- W.R. Gilks, S. Richardson, and D. Spiegelhalter. *Markov Chain Monte Carlo in Practice*. Chapman & Hall/CRC Interdisciplinary Statistics. Taylor & Francis, 1995.

- Matthew J. Beal. *Variational Algorithms for Approximate Bayesian Inference*. PhD thesis, Gatsby Computational Neuroscience Unit, University College London, 2003.
- John C. Butcher. *Numerical Methods for Ordinary Differential Equations*. John Wiley & Sons, third edition, 2016.
- E. Hairer, S. P. Nørsett, and G. Wanner. *Solving Ordinary Differential Equations I: Nonstiff Problems*. Springer, second edition, 1993.
- Kyle Cranmer, Johann Brehmer, and Gilles Louppe. The frontier of simulation-based inference. *Proceedings of the National Academy of Sciences*, 117(48):30055–30062, 2020.
- Mark Asch, Marc Bocquet, and Maëlle Nodet. *Data Assimilation*. Society for Industrial and Applied Mathematics, 2016.
- Mark A Beaumont, Wenyang Zhang, and David J Balding. Approximate bayesian computation in population genetics. *Genetics*, 162(4):2025–2035, 2002.
- Patrick R Conrad, Mark Girolami, Simo Särkkä, Andrew Stuart, and Konstantinos Zygalakis. Statistical analysis of differential equations: introducing probability measures on numerical solutions. *Statistics and Computing*, 27(4):1065–1082, 2017.
- Philipp Hennig, Michael A. Osborne, and Hans P. Kersting. *Probabilistic numerics : computation as machine learning*. Cambridge University Press, 2022.
- Jonas Beck, Nathanael Bosch, Michael Deistler, Kyra L. Kadhim, Jakob H. Macke, Philipp Hennig, and Philipp Berens. Diffusion tempering improves parameter estimation with probabilistic integrators for ordinary differential equations. In *The 41st International Conference on Machine Learning*, volume 235, 2024.
- H. Kersting, T. J. Sullivan, and P. Hennig. Convergence rates of gaussian ODE filters. *Statistics and Computing*, 30(6):1791–1816, 2020.
- Yvann Le Fay, Simo Särkkä, and Adrien Corenflos. Modelling pathwise uncertainty of stochastic differential equations samplers via probabilistic numerics. *Bayesian Analysis*, 1(1):1–24, 2025.
- Jonathan Schmidt, Nicholas Krämer, and Philipp Hennig. A probabilistic state space model for joint inference from differential equations and data. In *Advances in Neural Information Processing Systems*, volume 34. Curran Associates, Inc., 2021.
- M. Schober, S. Särkkä, and P. Hennig. A probabilistic model for the numerical solution of initial value problems. *Statistics and Computing*, 29(1):99–122, 2018.
- Filip Tronarp, Nathanael Bosch, and Philipp Hennig. Fenrir: Physics-enhanced regression for initial value problems. In *Proceedings of the 39th International Conference on Machine Learning*, volume 162, 2022.

- F. Tronarp, H. Kersting, S. Särkkä, and P. Hennig. Probabilistic solutions to ordinary differential equations as non-linear bayesian filtering: A new perspective. *Statistics and Computing*, 29(6):1297–1315, 2019.
- F. Tronarp, S. Särkkä, and P. Hennig. Bayesian ODE solvers: the maximum a posteriori estimate. *Statistics and Computing*, 31(3):23, 2021.
- Assyr Abdulle and Giacomo Garegnani. Random time step probabilistic methods for uncertainty quantification in chaotic and geometric numerical integration. *Statistics and Computing*, 30(4):907–932, 2020.
- Han Cheng Lie, Martin Stahn, and Timothy John Sullivan. Randomised one-step time integration methods for deterministic operator differential equations. *Calcolo*, 59(1):13, 2022.
- Han Cheng Lie, Andrew M Stuart, and Timothy John Sullivan. Strong convergence rates of probabilistic integrators for ordinary differential equations. *Statistics and Computing*, 29(6):1265–1283, 2019.
- Naoki Marumo, Takeru Matsuda, and Yuto Miyatake. Modelling the discretization error of initial value problems using the wishart distribution. *Applied Mathematics Letters*, 147:108833, 2024.
- Takeru Matsuda and Yuto Miyatake. Estimation of ordinary differential equation models with discretization error quantification. *SIAM/ASA Journal on Uncertainty Quantification*, 9(1):302–331, 2021.
- Yuto Miyatake, Kaoru Irie, and Takeru Matsuda. Quantifying uncertainty in the numerical integration of evolution equations based on Bayesian isotonic regression. *Japan Journal of Industrial and Applied Mathematics*, June 2025.
- Arnaud Doucet, Nando De Freitas, Neil James Gordon, et al. *Sequential Monte Carlo methods in practice*, volume 1. Springer, 2001.
- N.J. Gordon, D.J. Salmond, and A.F.M. Smith. Novel approach to nonlinear/non-gaussian bayesian state estimation. *IEE Proceedings F (Radar and Signal Processing)*, 140:107–113, 1993.
- Genshiro Kitagawa. Monte carlo filter and smoother for non-gaussian nonlinear state space models. *Journal of Computational and Graphical Statistics*, 5(1):1–25, 1996.
- Genshiro Kitagawa. A self-organizing state-space model. *Journal of the American Statistical Association*, 93:1203–1215, 1998.
- Nathanael Bosch, Adrien Corenflos, Fatemeh Yaghoobi, Filip Tronarp, Philipp Hennig, and Simo Särkkä. Parallel-in-time probabilistic numerical ode solvers. *Journal of Machine Learning Research*, 25(206):1–27, 2024.
- Jon Cockayne, Chris J Oates, Ilse CF Ipsen, and Mark Girolami. A bayesian conjugate gradient method (with discussion). *Bayesian Analysis*, 14(3):937–1012, 2019.
- Shinya Nakano, Genta Ueno, and Tomoyuki Higuchi. Merging particle filter for sequential data assimilation. *Nonlinear Processes in Geophysics*, 14(4):395–408, 2007.

- Peter Jan Van Leeuwen. Particle filtering in geophysical systems. *Monthly Weather Review*, 137(12): 4089–4114, 2009.
- Alban Farchi and Marc Bocquet. Comparison of local particle filters and new implementations. *Nonlinear Processes in Geophysics*, 25(4):765–807, 2018.
- Peter Jan Van Leeuwen, Hans R Künsch, Lars Nerger, Roland Potthast, and Sebastian Reich. Particle filters for high-dimensional geoscience applications: A review. *Quarterly Journal of the Royal Meteorological Society*, 145(723):2335–2365, 2019.
- Alexandros Beskos, Dan Crisan, and Ajay Jasra. On the stability of sequential Monte Carlo methods in high dimensions. *The Annals of Applied Probability*, 24(4):1396 – 1445, 2014.
- Radford M Neal. Sampling from multimodal distributions using tempered transitions. *Statistics and computing*, 6(4):353–366, 1996.
- Pierre Del Moral, Arnaud Doucet, and Ajay Jasra. Sequential monte carlo samplers. *Journal of the Royal Statistical Society Series B: Statistical Methodology*, 68(3):411–436, 2006.
- Ethan Atkins, Matthias Morzfeld, and Alexandre J Chorin. Implicit particle methods and their connection with variational data assimilation. *Monthly Weather Review*, 141(6):1786–1803, 2013.
- Alexandre Chorin, Matthias Morzfeld, and Xuemin Tu. Implicit particle filters for data assimilation. *Communications in Applied Mathematics and Computational Science*, 5(2):221–240, 2010.
- Arieh Iserles. *A First Course in the Numerical Analysis of Differential Equations*. Cambridge University Press, USA, 2nd edition, 2008.
- George Papamakarios and Iain Murray. Fast ε -free inference of simulation models with bayesian conditional density estimation. *Advances in neural information processing systems*, 29, 2016.
- Stefan T. Radev, Marvin Schmitt, Valentin Pratz, Umberto Picchini, Ullrich Köthe, and Paul-Christian Bürkner. Jana: Jointly amortized neural approximation of complex Bayesian models. In *Proceedings of the Thirty-Ninth Conference on Uncertainty in Artificial Intelligence*, volume 216, 2023.
- Jonas Bernhard Wildberger, Maximilian Dax, Simon Buchholz, Stephen R Green, Jakob H. Macke, and Bernhard Schölkopf. Flow matching for scalable simulation-based inference. In *Thirty-seventh Conference on Neural Information Processing Systems*, 2023.
- Manuel Gloeckler, Shoji Toyota, Kenji Fukumizu, and Jakob H. Macke. Compositional simulation-based inference for time series. In *The Thirteenth International Conference on Learning Representations*, 2025.
- Yuga Hikida, Ayush Bharti, Niall Jeffrey, and François-Xavier Briol. Multilevel neural simulation-based inference. In *Advances in Neural Information Processing Systems*, 2025.
- Rick Durrett. *Probability: theory and examples*, volume 49. Cambridge university press, 2019.